NUREG/CR-0865
PNL-2948
R-3

/-

Startup Data Report for NRC/PNL Halden Assembly IFA-513

D. D. Lanning
M. E. Cunningham

July 1979

Prepared for
the U.S. Nuclear Regulatory Commission

Pacific Northwest Laboratory
Operated for the U.S. Department of Energy
by Battelle Memorial Institute

Battelle

PNL-2948

NOTICE

PACIFIC NORTHWEST LABORATORY
operated by
BATTELLE
for the
UNITED STATES DEPARTMENT OF ENERGY
Under Contract EY-76-C-06-1830

Printed in the United States of America
Available from
National Technical Information Service
United States Department of Commerce
5285 Port Royal Road
Springfield, Virginia 22151

Price: Printed Copy $____*; Microfiche $3.00

*Pages	NTIS Selling Price
001-025	$4.00
026-050	$4.50
051-075	$5.25
076-100	$6.00
101-125	$6.50
126-150	$7.25
151-175	$8.00
176-200	$9.00
201-225	$9.25
226-250	$9.50
251-275	$10.75
276-300	$11.00

NUREG/CR-0865
PNL-2948
R-3

STARTUP DATA REPORT FOR NRC/PNL HALDEN ASSEMBLY IFA-513

D. D. Lanning
M. E. Cunningham

July 1979

Prepared for
The U.S. Nuclear Regulatory Commission
under a Related Services Agreement
with the U.S. Department of Energy
Contract EY-76-C-06-1830
FIN No. B-2043

Pacific Northwest Laboratory
Richland, Washington 99352

CONTENTS

TABLES

FIGURES

STARTUP DATA REPORT FOR NRC/PNL HALDEN ASSEMBLY IFA-513

INTRODUCTION

This report presents data from the first month of operation of IFA-513, which is a heavily instrumented 6-rod test assembly in the Halden Reactor in Norway. The assembly is jointly sponsored by the Halden Project and the Nuclear Regulatory Commission (NRC), and is part of a series of irradiation tests sponsored by the NRC to verify its single-rod fuel modeling computer programs. All the rods in the series are of the basic BWR-6 design with variations in gap size, fuel type, fill gas composition, and fill gas pressure.

The first two tests in the series were IFA-431 and IFA-432. These were identical 6-rod assemblies, each containing the same variations of gap size and fuel pellet types, but operating at different power levels and burnups. The present assembly, IFA-513, is the third in the series; its 6 rods are all identical, except for variations in fill gas composition and pressure. The fourth and last assembly, designated IFA-527, is yet to be built, and will study the effects of fuel pellet cracking and relocation.

The measurements made in IFA-513 and the earlier tests include:

- fuel temperature and power (both steady-state and transient)
- total cladding elongation, and
- fill gas pressure.

The above measurements are made on a continuous basis, providing a record of their variation with both power and burnup.

Along with the data, this report includes some analysis to put the IFA-513 startup data in perspective to similar data from IFA-431 and IFA-432.

ASSEMBLY DESCRIPTION AND INSTRUMENTATION

The IFA-513 assembly was designed with three purposes in mind:

1. to provide instrumented, irradiated rods, which are thoroughly characterized as to fabrication parameters and thermal history, for reuse in transient tests at the PBF reactor in Idaho Falls;
2. to extend the NRC Halden test series to include rods with known fill gas mixtures at several points between pure helium and pure xenon (and incidentally to check for segregation of those mixtures in-reactor) and
3. to quantify the variability among rods of contemporary design that have been fabricated identically and also operated identically.

The general design features of IFA-513, -527 and IFA-431, -432 are listed in Table 1. The specific variations for each rod in all four assemblies and the instrumentation for each rod is listed in Table 2. Figure 1 is a schematic of the IFA-513 assembly.

TABLE 1. General Design Characteristics For NRC/PNL Test Assemblies

Item	IFA-513, 527	IFA-431, 432
Number of Rods	6	6
Cladding:		
Material	Zircaloy-2	Zircaloy-2
ID x OD (m)	$1.09 \times 1.28 \times 10^{-2}$	$1.09 \times 1.28 \times 10^{-2}$
Tube Length (m)	0.824	0.61
Fuel Pellets:		
Material	UO_2	UO_2
Enrichment (%U-235)	9.9	10.0
ID x OD (m)	$0.175 \times 1.07 \times 10^{-2}$	$0.175 \times 1.07 \times 10^{-2}$
Pellet Length (m)	1.27×10^{-2}	1.27×10^{-2}
Active Pellet Column Length (m)	0.78	0.57
Pellet Density (%TD)	95	95, 92
Fuel Rod: Plenum Length (m)	2.9×10^{-2}	1.9×10^{-2}
Poison Pellet Length (each end) (m)	0.7×10^{-2}	0.7×10^{-2}

TABLE 2. Experimental Matrix

Assembly & Rod	Power[a] (kW/m)	Fuel[b] Type	Diametral Gap, M x 10^{-6}			Initial Fill Gas			Detectors[c]				SPND
			50-75	230	380	100% He 0.1 MPa	100% He >0.1 MPa	Xe 0.1 MPa	UTC	LTC	ES	PT	
IFA-431	35/25												7
1		95S		x		x			x	x	x	x	
2		95S			x	x			x	x	x		
3		95S	x			x			x	x	x		
4		95S		x				100%	x	x	x		
5		92S		x		x			x	x	x	x	
6		92U		x		x			x	x	x	x	
IFA-432	50/35												7
1		95S		x		x			x	x	x	x	
2		95S			x	x			UT	x	x		
3		95S	x			x			x	x	x		
4		95S		x				100%	x	x	x		
5		92S		x		x			x	x	x	x	
6		92U		x		x			x	x	x	x	
IFA-513	40/28												9
1		95S		x		x			x	x	x	x	
2		95S		x			0.3 MPa		x	x	x	x	
3		95S		x		x			x	x	x	x	
4		95S		x				8%	x	x	x	x	
5		95S		x		x			x	x	x	x	
6		95S		x				23%	x	x	x	x	
Fuel Relocation	14/10												9
1		95S	x					100%	x	x	x	x	
2		95S		x				100%	x	x	x	x	
3		95S		x				100%	x	x	x	x	
4		95S		x				100%	x	x	x	x	
5		95S		x				100%	x	x	x	x	
6		95S		x				100%	x	x	x	x	

(a) Linear power is given for upper and lower thermocouple positions respectively.
(b) Three fuel types are used, all enriched to 10% U-235.
95S = 95% TD, Stable
92S = 92% TD, Stable
92U = 92% TD, Unstable
(c) UTC = Upper Thermocouple
LTC = Lower Thermocouple
ES = Elongation Sensor
PT = Pressure Transducer
SPND = Self-Powered Neutron Detector
UT = Ultrasonic Thermometer

The major differences between IFA-513 and the two previous assemblies are as follows:

- Active fuel length of IFA-513 is 0.78 m; that of the previous assemblies is 0.57 m.
- The gas pressure transducers are installed on all 6 rods and are of a new type that continuously record pressure.
- Two extra vanadium self-powered neutron detectors are included between the top and bottom thermocouple planes to better define the axial flux shape.

As noted in Table 2, all fuel rods in IFA-513 are of the same fuel pellet type and the same fabricated gap size; the only variation is in the pressure and composition of the fill gas. Rods 1, 3, and 5 have pure helium fill gas at one atmosphere pressure (at room temperature). Rod 2 has helium fill gas at three atmospheres pressure, which is a new BWR design feature. Rods 4 and 6 have helium-xenon mixtures with 8% and 23% Xe, respectively, at one atmosphere pressure. The reason for the specific fractions chosen was to provide gas with a thermal conductivity approximately 75% and 50% that of pure helium.

The assembly design included special provision for the disconnection and reconnection of the thermocouple leads, so that individual rods might be reused (with instrumentation) in Power Burst Facility (PBF) transient tests.

The operation of the assembly has also been planned with its various purposes in mind. "Staircase" approaches to power throughout the life of the assembly have been requested so that the resistance-versus-power curve for each rod can be unequivocably defined. These curves have proven beneficial in analyzing the thermal performance.[1] Similarly, both linear and rapid power decreases have been requested on a periodic basis, since the resulting data can be used both to check the thermocouple performance and verify the steady-state data trends.[1,2]

The next section discusses preliminary data on temperature and power for the IFA-513 assembly.

POWER AND TEMPERATURE DATA

ASSEMBLY CALIBRATION AND ESTIMATE OF LOCAL POWER

The total assembly power is calculated by Halden from an average of the neutron detector readings, designated $\overline{ND}$:

Assembly power = KG ($\overline{ND}$), where KG is a calibration factor.[a]

The calibration factor is determined from a series of calibration runs during which the assembly power is held constant and the subcooling level of forced circulation coolant is varied. The subcooling power, Q_{sc}, is defined as the apparent assembly power determined from the coolant inlet flow and inlet/outlet temperature change. This figure only equals the assembly power when boiling is completely suppressed. Otherwise, a fraction of the assembly power is going to boiling water as well as heating water, and the actual assembly power is greater than Q_{sc}. The boiling power, Q_b, is determined from between the inlet and outlet flow rates, plus an assigned slip factor, which accounts for the differing flow rates of water and steam. The apparent subcooling power is corrected for heat inflow from the moderator, Q_m. Taking all this into account, we write:

$$Q_b + Q_{sc} - Q_m = Q_{assembly}$$

Halden has found that the most accurate way to find the true assembly power is to permit some boiling (to provide good coolant mixing), and to extrapolate a plot of Q_b versus $(Q_{sc} - Q_m)$ to Q_b equals 0. Such plots are shown in Figures 2, 3, and 4, which summarize the three calibration runs for IFA-513. Note that these runs were performed at approximately 100%, 50% and 40% of full power. Values for $\overline{ND}$ and estimated true assembly power are noted on the figures. From this data, a consistent value of 1.98 was found for KG.

(a) Halden calculates ND for IFA-513 by the following equation:

$$\overline{ND} = \frac{1}{2}\left[\frac{ND_1 + ND_2 + ND_3}{3\overline{ND}_1} + \frac{ND_6 + ND_7 + ND_8}{3\overline{ND}_6}\right]\left[\frac{ND_1 + ND_4 + ND_5 + ND_6}{4}\right]$$

It should be noted that the average values of $Q_{sc} - Q_m$ when boiling is suppressed (ramps 1 and 2) do not equal the extrapolated value. The difference is about 4.5%. It is felt that the zero-boiling data points are biased (possibly by poor coolant mixing), and therefore the extrapolated value is the more accurate. To get local power along the rod, Halden used to ratio the nearest single detector to the average ($\overline{ND}$), multiply by the average rod power and divide by the fuel length. Recently, however, Halden has corrected for radial flux tilting by translating the detector readings to the rod center lines prior to the final multiplication to get local power. In order to check the above method we took a somewhat different approach, the steps of which are listed below:

1. The detector readings at the thermocouple elevations were translated to the center line of the rods. At each elevation, the flux plane $\phi(x,y)$ was explicitly found in the form

   $$Ax + By + C = \phi$$

   To do this, we used the coplanar detector readings, together with their coordinates in x-y system with the assembly center as the origin. Then the value at each center line was calculated from the rod coordinates.

2. A similar operation was performed at the elevations of detectors 4 and 5. The upper flux plane function was presumed to apply at detector 5 elevation and the lower plane function at detector 4 elevation. The appropriate ratio (ND4/ND1 or ND5/ND6) was applied to the respective plane function.

3. Each rod was, therefore, characterized with 4 pseudo neutron detector readings evaluated at the rod center line at the 4 elevations of the flux measurement. The flux was presumed to vary linearly between points of measurement.

4. The flux variation seen by the fuel below the lower thermocouple was estimated by extrapolating to zero flux at the core base plate. The flux for the fuel above the upper thermocouple was extrapolated from the previous segment.

5. The flux along each rod was integrated with respect to axial length.

6. The flux integrals for all six rods were summed. The calibration factor (CALIB) was defined as the ratio of the assembly power to the sum of integrals.

7. The heat ratings at thermocouple sites were calculated directly by multiplying CALIB times the pseudo reading at that site.

Because we were handling large amounts of data, these steps were programmed into a computer. The linear heating ratings calculated by this method compare within 1.5% to the Halden values when the Halden-quoted assembly power is used to establish CALIB.

TEMPERATURE AND RESISTANCE DATA

Rather than plotting temperature versus power, we have found it both convenient and more revealing to plot resistance versus power, where resistance, R, is defined by:

$$R = \frac{T_{center} - T_{coolant}}{Power}$$

The various advantages of this form of data plot are discussed in Reference 1. In brief, the major convenience is that the relationship of temperature to power can be summarized for a broad range of power by a single number. Furthermore, the curvature of the resistance-versus-power plot is correlated to the "state" of the rod, e.g., whether it is in firm contact with the cladding. The transition power range from little or no fuel-cladding contact to firm contact is easier to determine from a resistance-power plot than from a temperature-power plot.

Resistance data is plotted versus power for all six IFA-513 rods in Figures 5-10. The data comes from the first two weeks of operation. The least squares-fit curves for the rods are brought together in Figure 11. The startup resistance ranges at specific powers for the 230μ-gap helium-filled rods from IFA-431 and 432 are also noted in Figure 11. The resistances of the helium- filled IFA-513 rods are very nearly the same as their counterparts from the earlier tests. The resistance variability of these 230μ-gap,

helium-filled rods is also much less at the high-power, upper thermocouple locations than at the low-power, lower thermocouple locations. This is probably because there is simply less gap (at power) in the higher-power locations. Finally, it appears that the additional helium pressure in rod 2 does not significantly change its resistance.

The mixed-gas IFA-513 rods display resistances somewhat higher than the helium-filled rods, which is to be expected due to their degraded gas conductivity. However, as the following discussion will show, the magnitude of the resistance increase is not what would be expected from either simplistic assumptions or current NRC computer codes.

The basis for discussion is Figure 12, which is a plot of resistance data taken from selected IFA-431, -432, and -513 rods at the upper thermocouple locations at 35.0 kW/m. The abscissa of the plot is the conductivity of the fill gas (at power) relative to that of pure helium. Figure 12 shows upper thermocouple resistance data for all of the IFA-513 rods, together with the data from Rods 1 and 4 of IFA-431, -432. Rod 1 in each assembly was helium-filled and had a 230μ-gap. Rod 4 of IFA-432 had the same gap size but was filled with pure xenon.

The average gap size for the helium-filled rods can be inferred by applying the following reasoning (the same as that employed with GAPCON, FRAPCON, and other related codes).

1. With radial heat flow only, the fuel surface temperature T_{FS} can be inferred from the relation

$$\int_{T_{FS}}^{T_{center}} K dT = \frac{qf}{4\pi}$$

where q is the local power (kW/m) and f is the "flux depression factor" ≈0.835 for the annular 10% enriched pellets under discussion.

2. The cladding inner surface temperature can be estimated from the relation

$$T_{CI} = T_{coolant} + \frac{q}{2\pi r_{CS} h_f} + \frac{q \quad \ln (r_{CS}/r_{CI})}{2\pi K_c}$$

where r_{CS}, r_{CI} are cladding outer and inner radii, respectively,
h_f is film coefficient, and
K_c is thermal conductivity of cladding at average temperature

3. The gap conductance can now be calculated as

$$h_{gap} = \frac{q}{2\pi r_{FS} (T_{FS} - T_{CI})}$$

4. The effective gap size is given by

$$K_{gas}/h_{gap} = d_{eff},$$

where K_{gas} is the gas thermal conductivity.

5. The physical gap size is given by

$$d_{phys} = d_{eff} - g_1 - g_2$$

where g_1 and g_2 are the temperature jump distances at the two surfaces.

For an average resistance of 2.7×10^{-2} K-m/W, $T_{center} = 1185^{o}C$ at 35.0 kW/m. The effective gap size is 34.1μm when the assumptions listed in Table 3 are used. If we assumed that this gap size did not change, effective resistance versus gas conductivity would be reflected by the dashed curve plotted in Figure 12. This curve far overpredicts the resistance at low gas conductivity. Apparently the gap size at low conductivity is much <u>less</u> than the 34μm we assumed. We conclude that the reduction of the gap with increasing fuel temperature must be accounted for.

TABLE 3. Assumptions Used to Infer Gap Size From IFA-513 Data

Item	Model or Assumption	Value
Fuel Thermal Conductivity	Lyons Equation[3] for 95% TD UO_2	-
Flux depression factor (f)	BRT-1 Code[4]	0.8346
Film Coefficient (h_f)	Jens-Lottes Correlation	50 kW/m^2-K
Conductivity of He at ~380°C (h_{gap})	Chapman-Enscog,[5] modified by Wilke	0.26 W/m-K
Conductivity of Zry-2 at ~280°C ($\overline{K}_c$)	Data of Scott[6]	15 W/m-K
$T_{coolant}$	Halden Standard Operating Conditions	513K
Temperature Jump Distance ($g_1 + g_2$) at ~380°C for He at 0.2 MPa	GAPCON-2 Model[7]	5.4μm

Thus, we should use a fuel modeling code to estimate the gas effect. The results from the NRC code GAPCON-3[8] are also plotted in Figure 12 for the case of no relocation assumed in the calculation. It, too, overpredicts the data although not so severely as hand calculations with the simplistic assumption of no gap closure. This indicates that both thermal expansion and relocation are closing the gap. The same is indicated by FRAPCON-1.[9]

TRANSIENT RESPONSE OF THE RODS

Two types of transients have been performed: a linear power decrease at a rate of 0.36%/sec, and fast power decreases at rates greater than 1.3%/sec.

We will consider the results of the "linear" power decrease first. As Lanning has stated,[1,2] the linear power decrease can be used to verify steady state resistance trends, at least qualitatively, and the cross-check is quantitative if the power change is truly linear with time.

The normalized cobalt self-powered neutron detector (SPND) readings from the first linear power decrease for IFA-513 (run 117) are plotted in Figure 13, together with the normalized temperatures from the lower thermocouples of rods 1, 2, and 6. As indicated in Reference 1, the ratio of temperature and power slopes is connected to the resistance-versus-power (R-vs-P) behavior. Furthermore, this correlation applies to calculated slope ratios as well, and is little affected by the model chosen to make the calculation. Thus, by comparing calculated and measured normalized slope ratios, we can make a good cross-check on the accuracy of the initial thermocouple reading, which is the normalization constant.

Figure 11 shows the tendency of R-vs-P curves for the thermocouples to be quite flat. Thus, we would expect the slope ratios for the thermocouples to be close to 1.0. This expectation is confirmed by the slope ratio data recorded in Table 4.*

TABLE 4. Results for Linear Power Decrease (Run 117)
(Power Slope = 0.34%/sec)

Rod Number	Thermocouple	Measured Slope Ratio[a]	Calculated Slope Ratio[a,b]
1	upper	1.06	1.13
1	lower	1.10	1.05
2	lower	1.06	1.02
3	lower	1.08	1.06
4	upper	1.11	1.17
4	lower	1.05	1.04
5	upper	1.05	1.12
5	lower	1.08	1.05
6	upper	1.08	1.15
6	lower	1.00	0.971

(a) All measured and calculated values have a standard deviation of 0.04 (1σ).
(b) The calculated slope ratios were gained from inputting the IFA-513 rod design, the measured R-vs-P behavior, and the measured Run 117 power history to the transient temperature calculator MWRAM, which is described in Reference 1.

*These numbers are "close" to 1.0, relative to the maximum possible range for the slope ratio, which is from $\sim$0.50 to 1.30.

Calculated slope ratios for the various thermocouples are also recorded in Table 4. The agreement between calculated and measured values is within experimental error in most cases, thus confirming the thermocouple readings. There is a chronic trend in the data, however, which is somewhat disturbing; the measured slope ratio values for the lower thermocouples are in every case larger than the calculated values, while the opposite is true for the upper thermocouples. There are at least two possible causes for this:

- The centrally located cobalt detector may only approximate the change in relative power at the thermocouple locations. The actual change in relative power may not be uniform along the length of the assembly. A 1% discrepancy in the relative power change translates to a 5% discrepancy in slope ratio estimation for 20% power drops (1%/20% = 5%).
- The power change in this run is by no means perfectly linear. This reintroduces some model dependency on the calculated slope ratio values.

The first of these causes is the most likely, and is certainly most likely to be apparent in IFA-513 than in the shorter previous assemblies.

Now let us consider the results from fast power drops. We have found a way to plot data from these runs that is both highly revealing as to the probable modes of heat transfer in the rod and relatively independent of the effective thermocouple time constant. The quantity to be plotted against time is $-\ln(T_N-a)$, where "a" is the ratio of power before and after the step, and T_N is the normalized temperature defined earlier.

In the limit of an ideal step decrease and no temperature dependence of thermal parameters, calculated plots of $-\ln(T_N-a)$ versus time are straight lines. The slopes of the lines are highly characteristic of the total resistance and somewhat sensitive to the partition in resistance between fuel and gap. The slopes are totally independent of the thermocouple time constant.

When temperature dependence of thermal parameters is considered, calculated plots of $-\ln(T_N-a)$ are no longer straight lines. However, the departure of the plots from linearity is characteristic of the heat transfer modes

assumed in the model, and the curvatures of the plots have been shown to be quite independent of the thermocouple time constant.

The fact that the "fast" power decreases provided by Halden are by no means quick, clean, step drops frustrates forming a quantitative statement about heat transfer modes based on current data. But qualitative conclusions are well confirmed, as will be shown.

Consider for example, two extreme views of heat transfer in the fuel rod:

Model 1: In this model there are no fuel cracks. This means there are no crack-caused impediments to radial heat flow. The conductivity is considered to be of the Lyons form[3] for 95% dense UO_2. The changes in gap conductance with power are assumed to be dominated by the thermal expansion of the fuel and cladding, which in turn is related to their respective temperatures.

Model 2: In this model, the fuel has many small and randomly oriented cracks. This results in impediments to the radial flow of heat, which can be accounted for by a temperature-dependent multiplier on the fuel thermal conductivity. The fuel is envisioned to be fully relocated to the cladding, so that over the range of the power decrease there is little change in the gap conductance. The change in resistance with power is presumed to be totally due to the change in effective conductivity, dominated by the crack factor.

Each of these two models can be adjusted to match a particular R-vs-P plot. Once so adjusted, they will produce nearly identical estimates of normalized temperature/power slope ratio during a linear power decrease. Thus neither steady-state data nor linear power decrease provides much information as to which is closer to the real heat transfer in the fuel rod. But these models do not produce the same cladding temperatures in LOCA-type calculations so it is important to know which is correct. A possible answer can be found by examining the fast-drop data.

A few days after the assembly was first brought to power, a typical fast power drop of 20% in 15 seconds was performed. A plot of the normalized power for this case (Run 115) is shown in Figure 14. We will concentrate on the data from this run for Rod 6 (23% Xe, 77% He fill gas) since, with its low gas conductivity, this rod is the most sensitive to assumptions about fuel cladding gap size and gap size changes.

A plot of $-\ln(T_N-a)$ is shown for the upper thermocouple location of Rod 6 for Run 115 in Figure 15. Also shown in Figure 15 are MWRAM-calculated responses using both model 1 and model 2.[(a)] It is evident in Figure 15 that model 2 is doing a much better job than model 1 in matching the data slope. Figure 16 illustrates this more graphically: the absolute calculated versus measured differences are plotted versus time. One should expect a rather constant difference (based on equality of curvature) in the time range from about 15 to 25 seconds if the model is correct. The information in Figure 17 indicates that, if model 2 is retained but the conductance is increased to 10.0 kW/m^2-K (with corresponding adjustment to the fuel conductivity) the agreement is even better.

The transient data thus indicates that the fuel is in firm contact with the cladding (light contact would only produce a conductance of $\sim$2.0 kW/m^2) and that the effective fuel conductivity is significantly degraded. The elongation data for this rod at this time, interestingly enough, shows definite pellet-cladding interaction, which further supports the conclusions from the transient data.

Next to be considered is the data from the lower thermocouple of Rod 6. The data and calculations of models 1 and 2 are shown in a $-\ln(T_N-a)$ plot in Figure 18. Again we see that model 2 matches the data curvature far better than model 1. However, no contact or only light contact is indicated (see Figure 19).

(a) Both tuned to resistance-power (R-P) data for Rod 6.

The helium-filled rods are less sensitive to the different assumptions about gap size, but some surprisingly definite concludions seem evident from the helium-rod data. First, the lower thermocouples all operated at low power and (due to the helium fill) at center line temperatures below 1100°C. In these relatively benign conditions the pellets appear to retain enough integrity to shrink, such that the gap widens upon power decrease, and model 1 seems more appropriate than model 2 (Figures 20-23).[a] On the other hand, the upper thermocouple location, which operated at center line temperatures in excess of 1400°C, appears to have cracked more, making model 2 more appropriate (Figures 24 and 25). The conductance distinction between light and heavy contact is much less for a helium-filled rod than for Rod 6 such that a prediction about interaction between pellet and cladding (PCI) is not possible on the basis of this data. However all the He rods did evidence PCI on the first power rise, as indicated in cladding elongation vs power plots.

In summary, the linear power decrease does provide confirmation of the thermocouple readings--within experimental error. The fast power decreases have led to tentative conclusions about fuel structure and heat transfer modes which are at variance with current thermal performance modeling, but which nonetheless are valid.

(a) Particularly in Figure 20 (Rod 1) we see that the model 1 difference between measured and calculated values is constant, whereas the model 2 difference continually increases. Again, the more correct model should achieve a constant measured-calculated difference.

CLADDING ELONGATION AND GAS PRESSURE DATA

CLADDING ELONGATION MEASUREMENTS

The total elongation of the cladding is continuously measured by a linear variable displacement transducer (LVDT) at the lower end of each rod. The rods are laterally supported as they hang in the assembly. Thus, in the absence of coolant temperature changes with power, which might expand or contract the stay rods, the LVDT reading should be a direct indication of cladding elongation.

The occurrence of pellet-cladding mechanical interaction (PCMI) can be estimated by a departure of the cladding elongation from that expected on the basis of cladding expansion alone. Thus, the estimate of cladding axial expansion is an integral part of the analysis of cladding elongation data. Because the fuel rod has an axial power profile, cladding elongation can be estimated by summing estimates of expansion for various sections of the total cladding tube. These calculations are tedious, and therefore, a computerized approach was taken:

1. The computer program developed to test the assembly and local powers was used to develop 6-point power profiles of each rod at each 15-minute time step of a power ramp.
2. Previous to the calculation of power, the vanadium SPND readings were corrected for time lag by a device recently developed for another program.
3. The peak powers and power profiles and times were input to the GAPCON-3 computer program (which can handle time-varying axial profiles). The GAPCON-3 program was modified to include the MATPRO-10 functions for zircaloy expansion.

Results of this exercise for the first rise to power for the assembly are presented in Figures 26-30. The solid lines are the estimated total cladding elongation due to thermal expansion ($\pm$10%). The dots are the measured elongation. All rods show some evidence of PCI, although rod 6 shows the strongest elongation. The relaxation of elongation after each power step is also evident.

The elongation data for rod 1 for the next two power ramps are shown in Figures 31 and 32. The zero-power elongation detector reading has shifted upward for some unknown reason. Accordingly the calculated estimate of cladding elongation is set up to this same point. The measured elongation now diverges from the corresponding calculated value for thermal expansion alone. The reason for this behavior is not clear, but it repeated in both ramps by rods 1-5. The elongation behavior of rod 6 in these two power ramps is shown in Figures 33 and 34. Again, there is a scale shift and a diminution of the signal, but the slope of the elongation versus time is still greater than the slope of expansion versus time, indicating some PCI.

GAS PRESSURE MEASUREMENTS

There are two trends of interest with respect to the gas pressure measurements: the change in pressure as a function of power and as a function of burnup. From the startup data, we only have the gas pressure as a function of power.

We have compared the calculated volumes within the fuel rods to the measured free volume found at Kjeller, and we conclude that the following apportionment of the volume (in cm^3) holds approximately for all 6 rods:

Plenum volume (with spring)	2.5
Gap volume	3.3
Pressure detector volume	3.0
Total	8.8 cm^3

The decrease in volume of this system going from room temperature to hot standby (zero power) at 240°C is negligible. The expected pressure at zero power can thus be calculated directly from the ratio of Kelvin temperatures.

$$1 \times 0.1013 \times \frac{533}{293} = 0.1843 \text{ MPa for rods 1, 3-6}$$

$$3 \times 0.1013 \times \frac{533}{293} = 0.5530 \text{ MPa for rod 2}$$

Halden has adjusted the reported values to match the above, by additive constants. In the case of rod 2, the correction is very large (0.20 MPa).

The relative measured increase in pressure for Ramp 1 is shown in Figure 35 for rods 2 and 6. The average increase at full power is about a factor of 1.25, with rod 6 increasing the most, as would be expected from its higher fuel temperatures. To check the reasonableness of this measured increase, GAPCON-3 was run with the IFA-513 design as input.

The calculated relative pressure increase was 20%, which is fairly close to the measured value.

SUMMARY

The startup of IFA-513 was generally very successful. Five of the 33 measurement instruments failed on startup: two upper fuel centerline thermocouples, two pressure transducers, and one cladding elongation sensor. The loss of this instrumentation, however, did not seriously impair the test.

Initial centerline temperature and power data is highly consistent with that from previous tests. The new data emphasizes again the conservatism of both FRAPCON-1 and GAPCON-3 with respect to fuel temperatures. Transient temperatures from linear power decreases confirm the steady-state resistance versus power curves. The transient temperatures from fast power decreases definitely indicate higher conductances and lower effective fuel conductivity than those presumed by GAPCON-3.

Cladding elongation and gas pressure measurements are generally following expected trends as a function of rod power.

REFERENCES

1. D. D. Lanning, B. O. Barnes, and C. R. Hann, Manifestations of Non-Linearity in Fuel Center Line Thermocouple Steady-State and Transient Data: Implications for Data Analysis, NUREG/CR-0220, PNL-2602, Pacific Northwest Laboratory, Richland, WA 99352, January 1979.

2. D. D. Lanning, "Qualitative Confirmation of Steady-State Fuel Center Line Thermocouple Data from Transient Response" ANS Transactions, Volume 30, November 1978.

3. M. F. Lyons, et al., UO_2 Pellet Thermal Conductivity from Irradiation with Central Melting, GEAP-4624, Advanced Reactor Studies, Nuclear, General Electric Company, Sunnyvale, CA 94086, 1964.

4. L. J. Page and D. R. Skeen, THERMOS/BATTELLE; The Battelle Version of the THERMOS Code, BNWL-516, Pacific Northwest Laboratory, Richland, WA 99352, 1967.

5. R. B. Bird, W. F. Stewart, and E. N. Lightfoot, Transport Phenomena, John Wiley & Sons, New York, 1966.

6. D. B. Scott, Physical and Mechanical Properties of Zircaloy-2 and Zircaloy-4, WACAP-3629-41, Westinghouse Electric Corp., Pittsburgh, PA 15235, 1965.

7. D. D. Lanning and C. R. Hann, Review of Methods Applicable to the Calculation of Gap Conductance in Zircaloy-Clad UO_2 Fuel Rods, BNWL-1894, Pacific Northwest Laboratory, Richland, WA 99352, 1975.

8. D. D. Lanning, B. O. Barnes and A. R. Olson, "Use of Fuel Thermocouple Transient Response for Data Verification and Fuel Rod Modeling." Article submitted to Nuclear Technology, May, 1979.

9. G. A. Berna et al., FRAPCON-1: A Computer Code for the Steady-State Analysis of Oxide Fuel Rods, CDAP-TR-78-032, EG&G Inc., Idaho Falls, ID 83401, 1978.

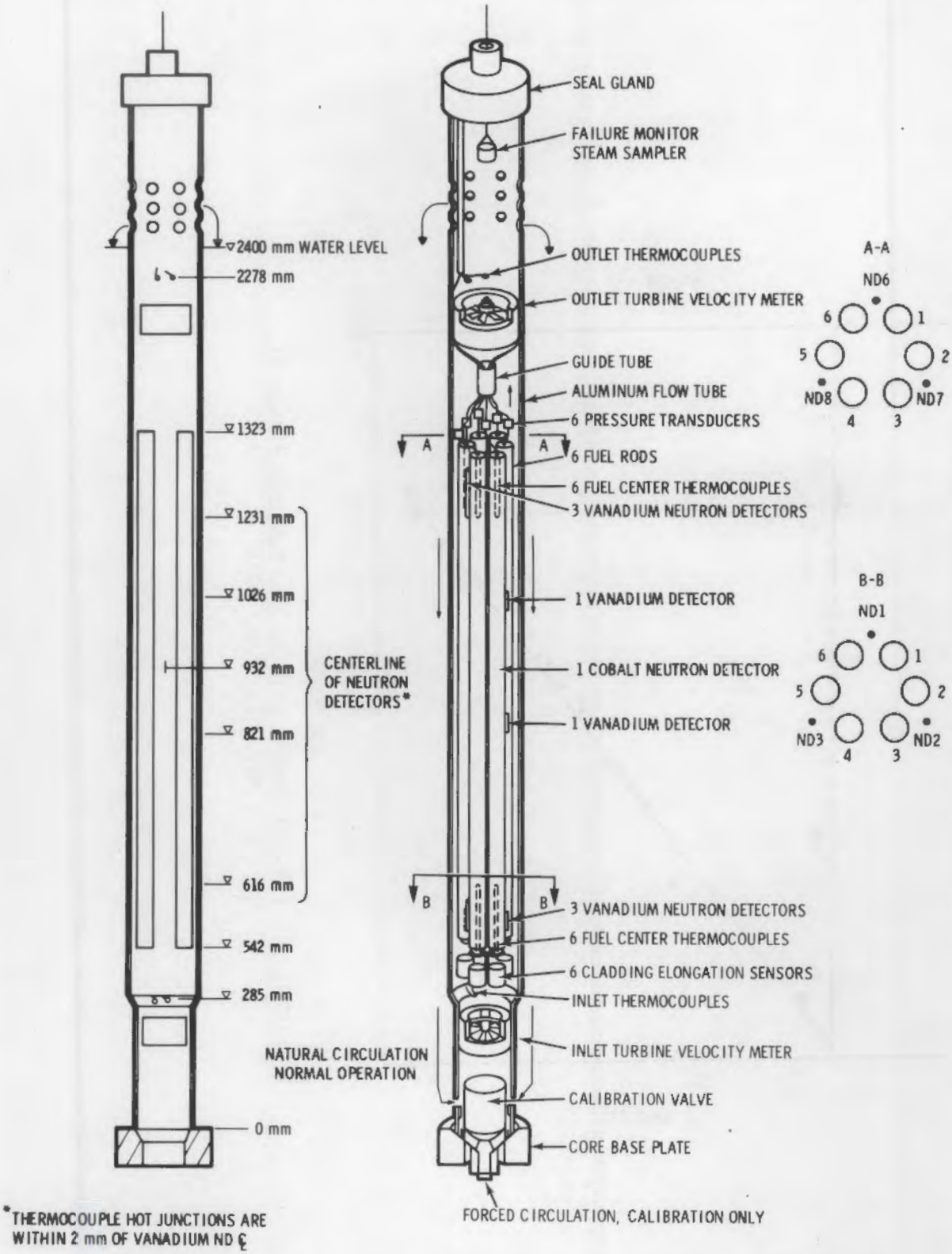

FIGURE 1. Schematic Design of IFA-513. (Note that neutron detectors 4 and 5 are in line with detectors 1 and 6.)

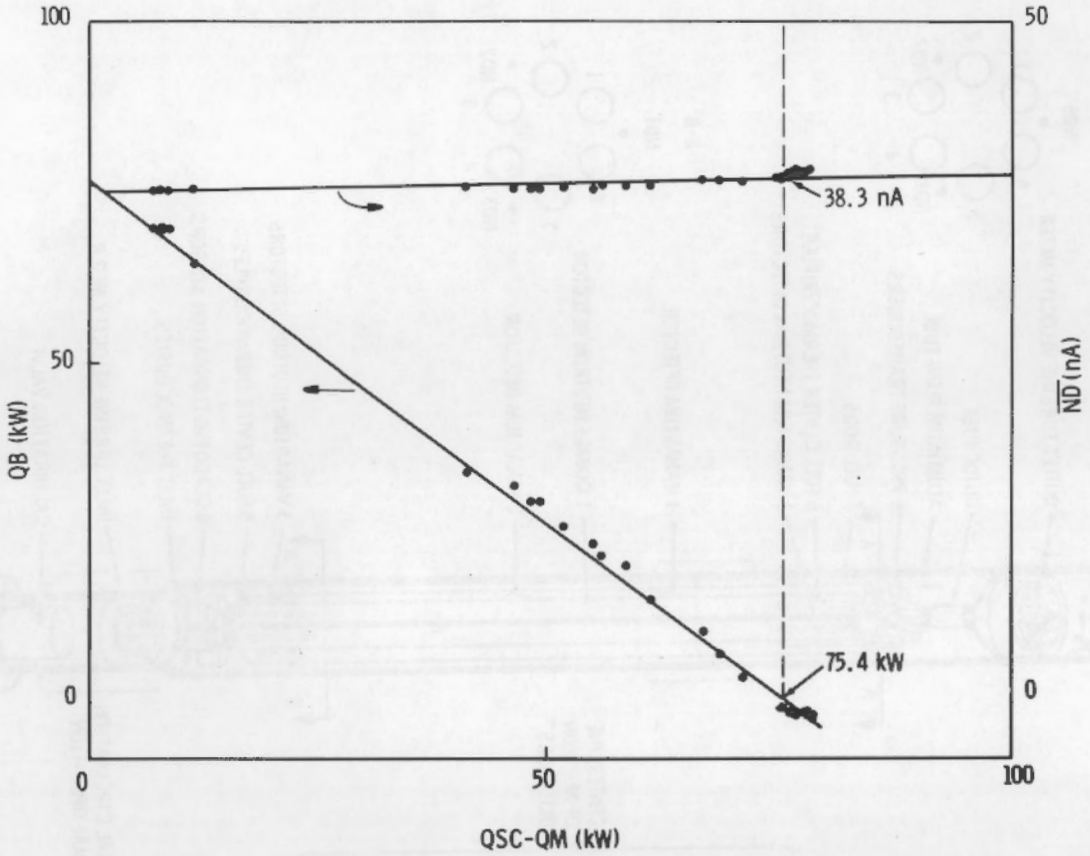

FIGURE 2. IFA-513 Power Calibration, Subcooled Ramp #1, QR - 6.1 MW, 3 December 1978

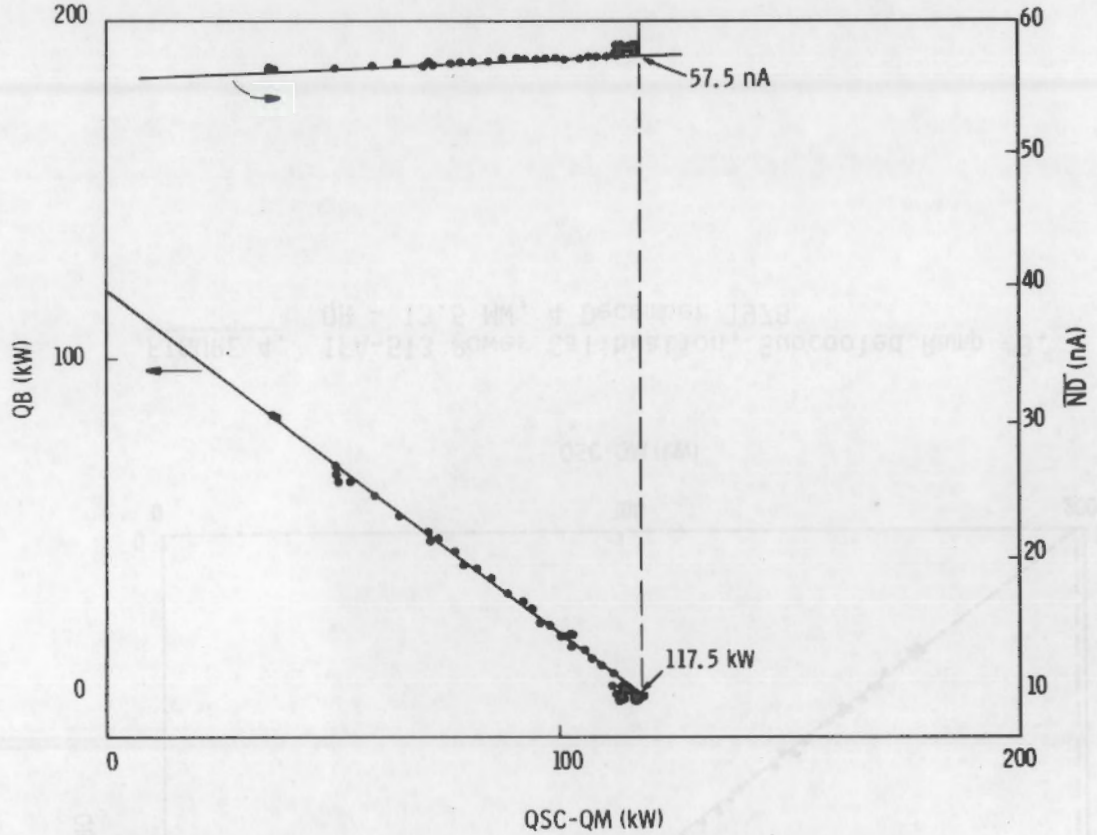

FIGURE 3. IFA-513 Power Calibration, Subcooled Ramp #2, QR - 8.4 MW, 3 December 1978

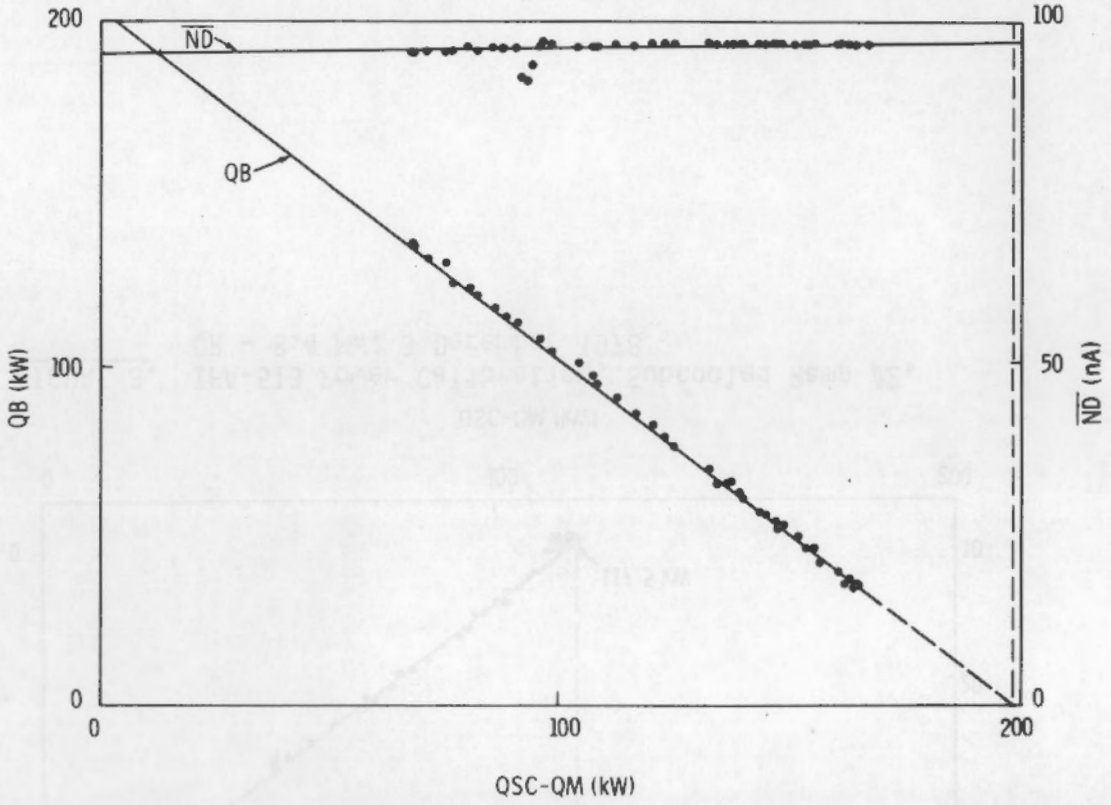

FIGURE 4. IFA-513 Power Calibration, Subcooled Ramp #3, QR - 13.6 MW, 4 December 1978

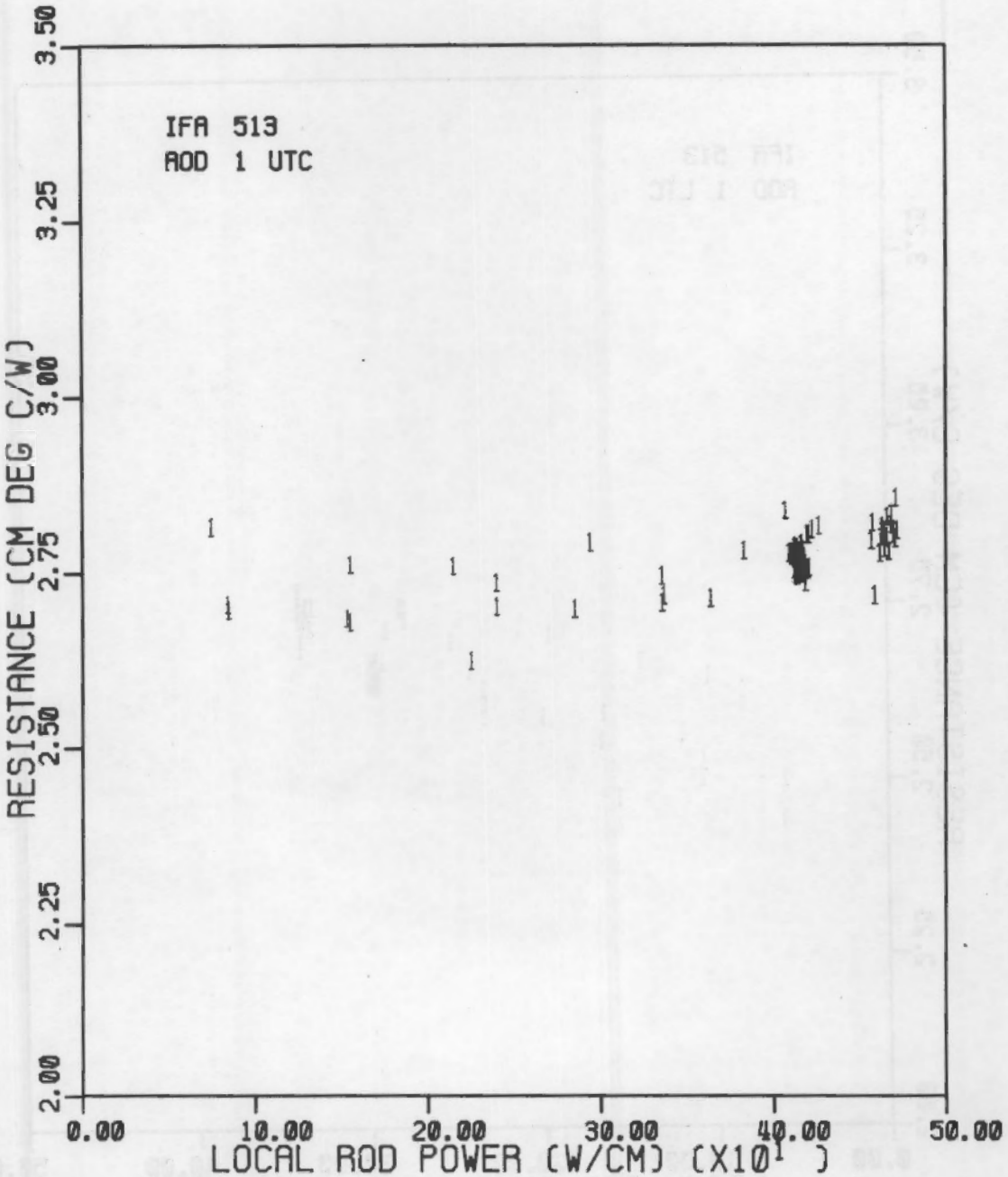

FIGURE 5a. Resistance vs. Power Data for Rod 1, upper Thermocouple.

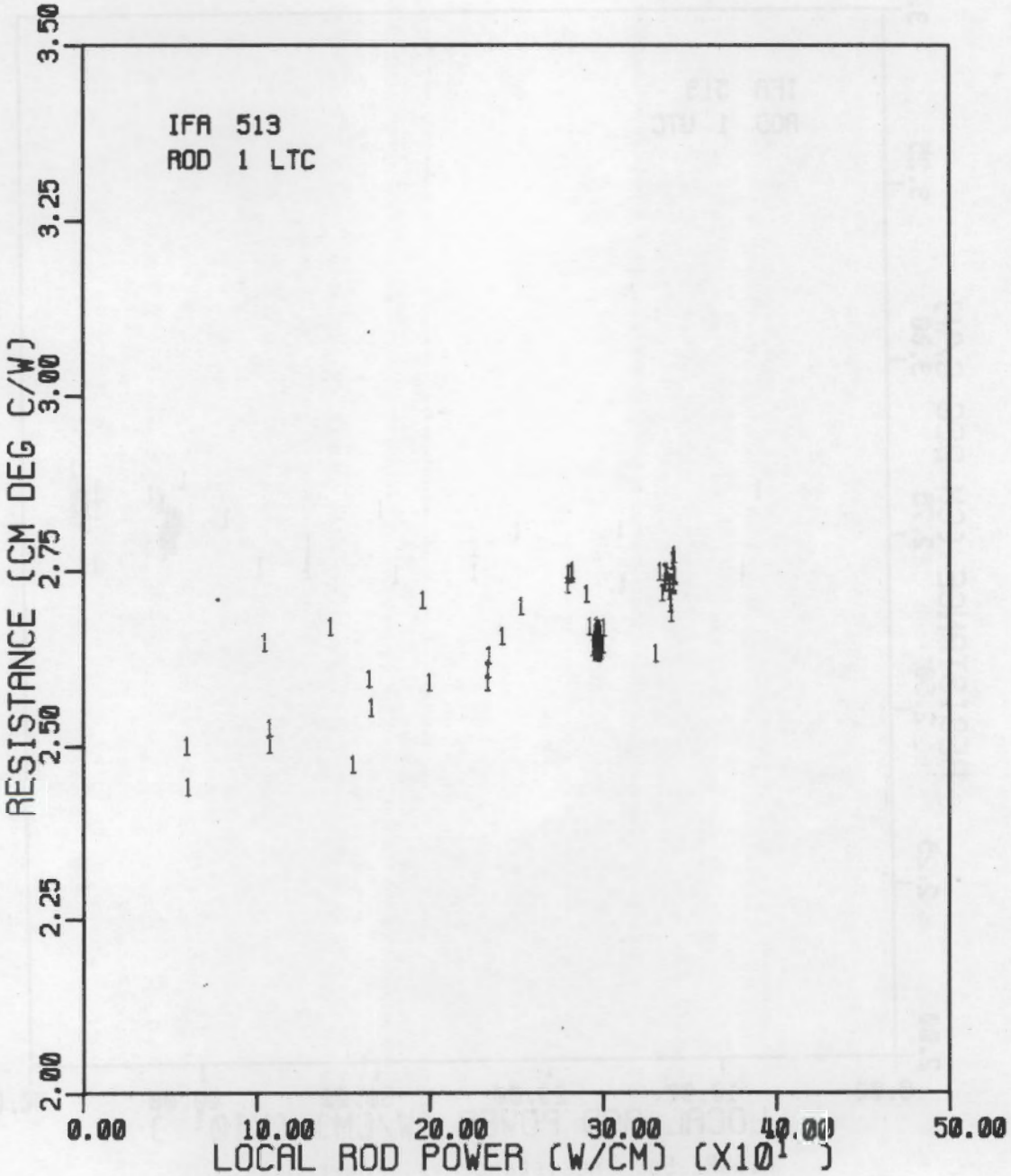

FIGURE 5b. Resistance vs. Power Data For Rod 1, Lower Thermocouple.

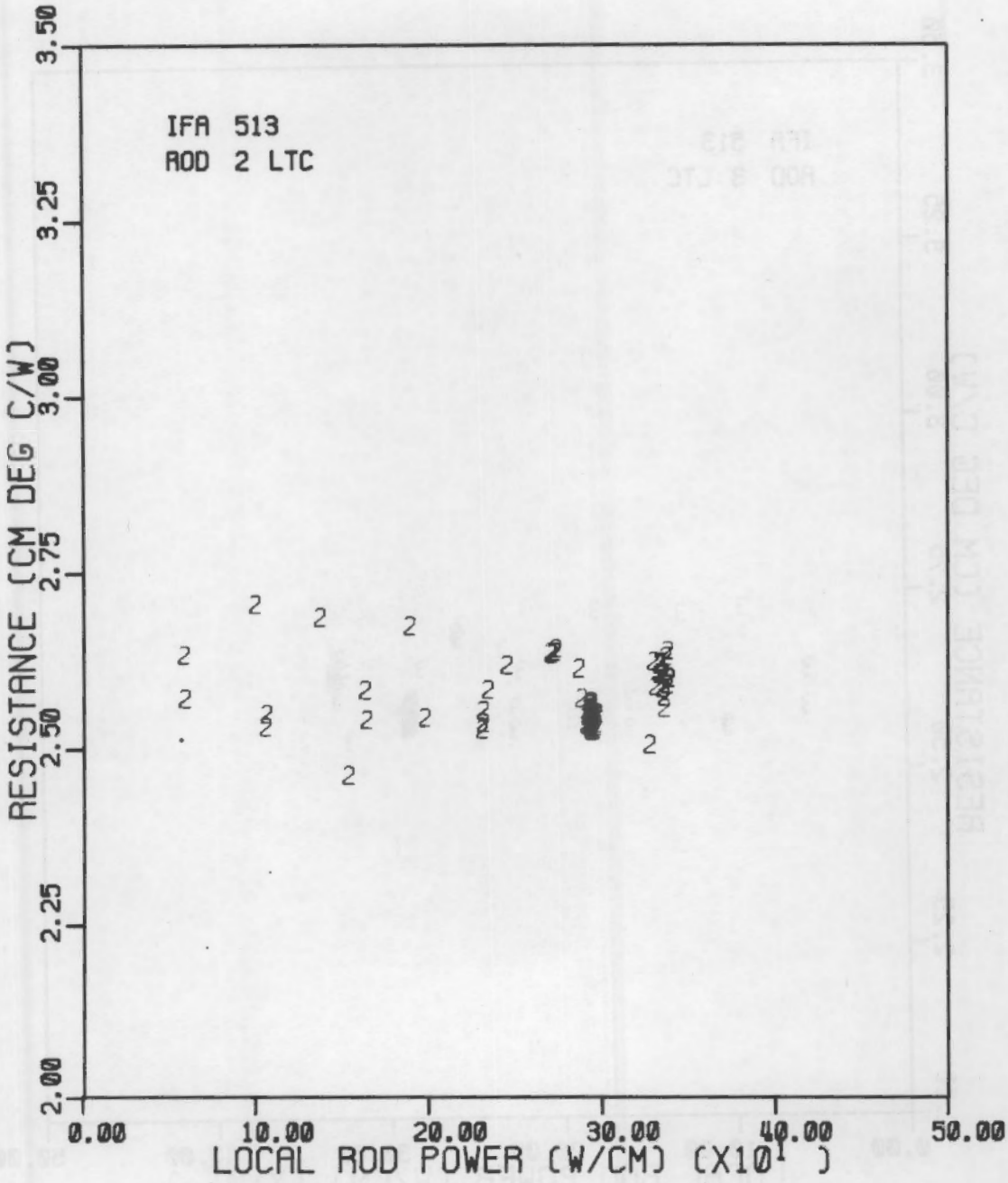

FIGURE 6. Resistance vs. Power Data
For Rod 2, Lower Thermocouple.

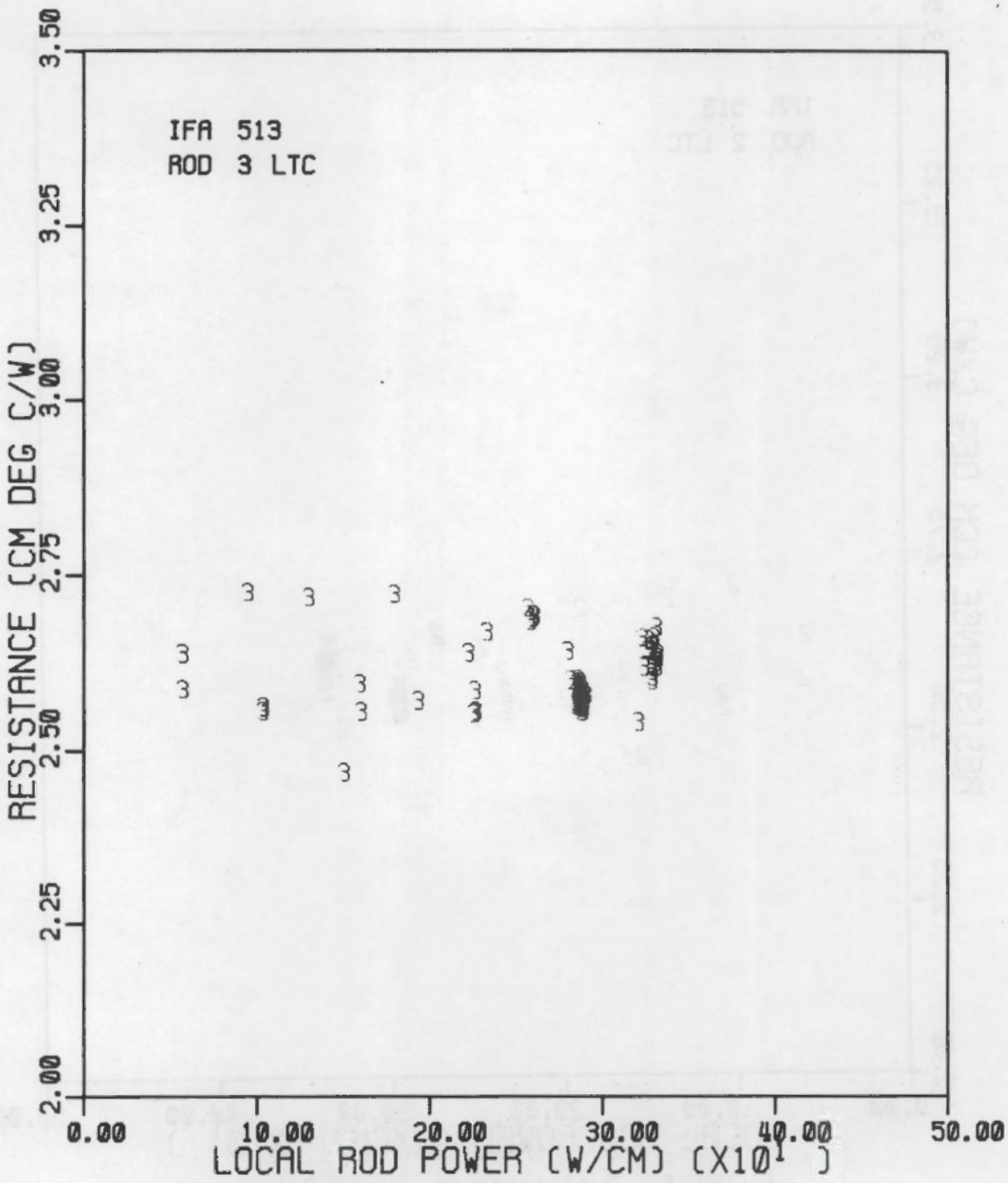

FIGURE 7. Resistance vs. Power Data For Rod 3, Lower Thermocouple.

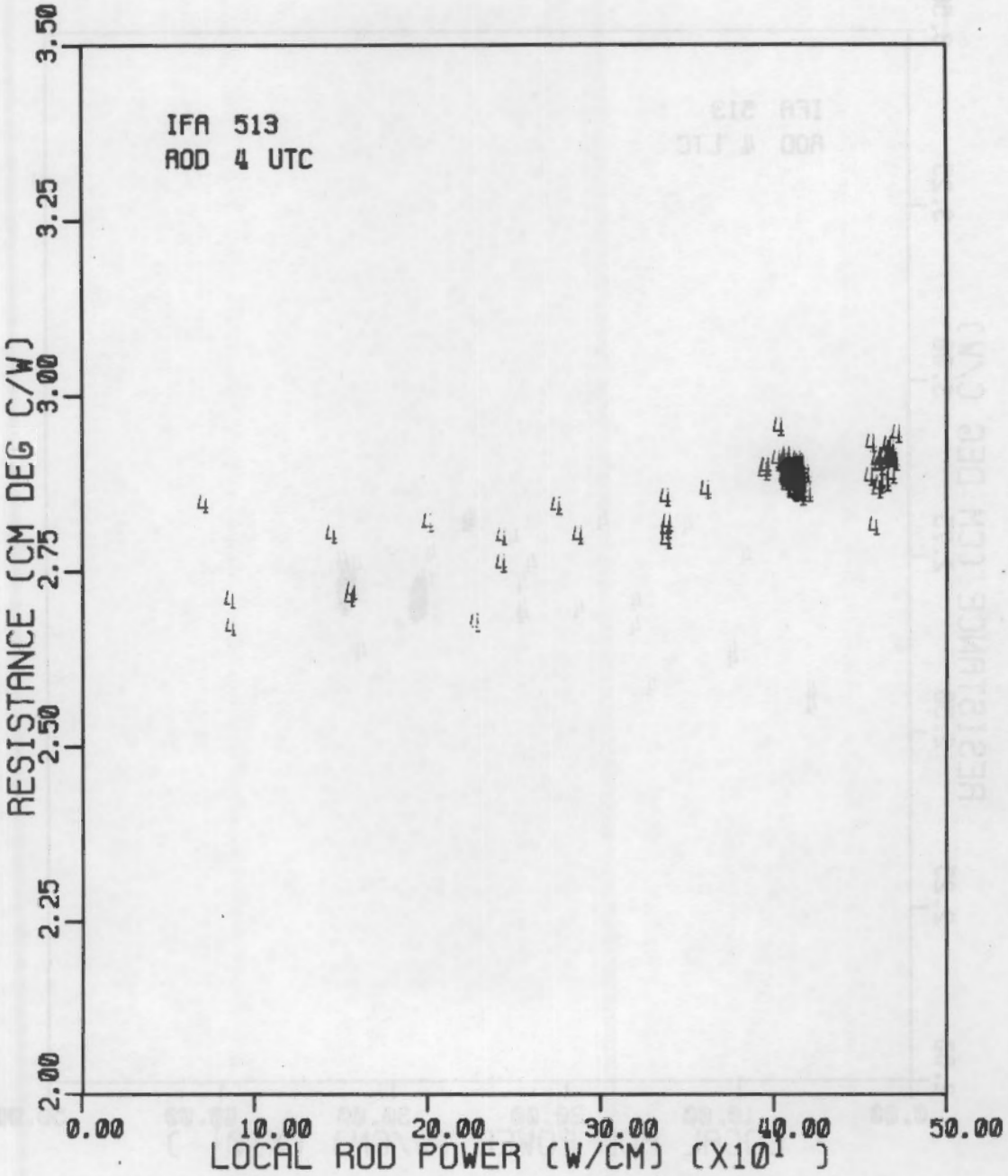

FIGURE 8a. Resistance vs. Power Data For Rod 4, Upper Thermocouple.

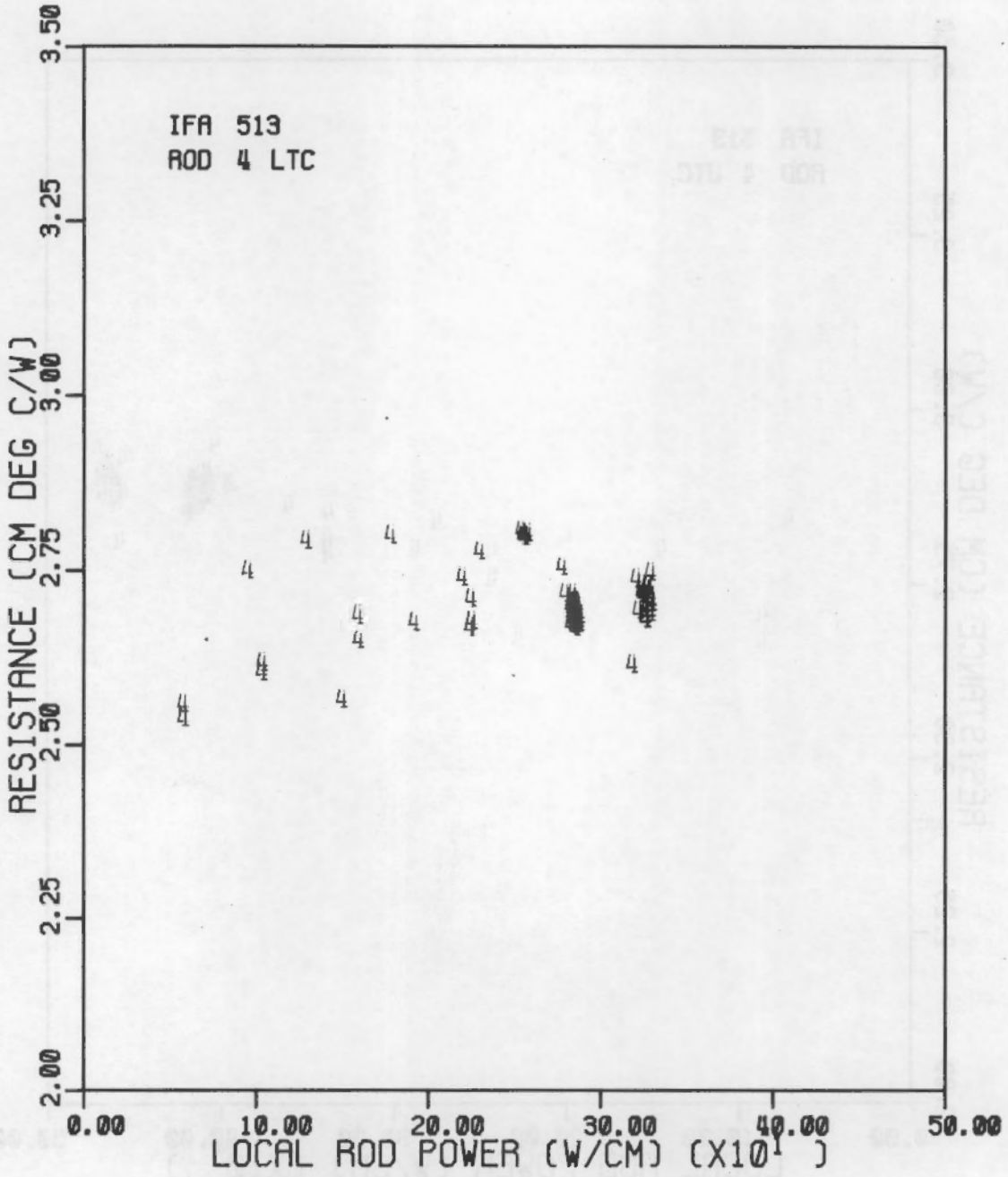

FIGURE 8b. Resistance vs. Power Data For Rod 4, Lower Thermocouple.

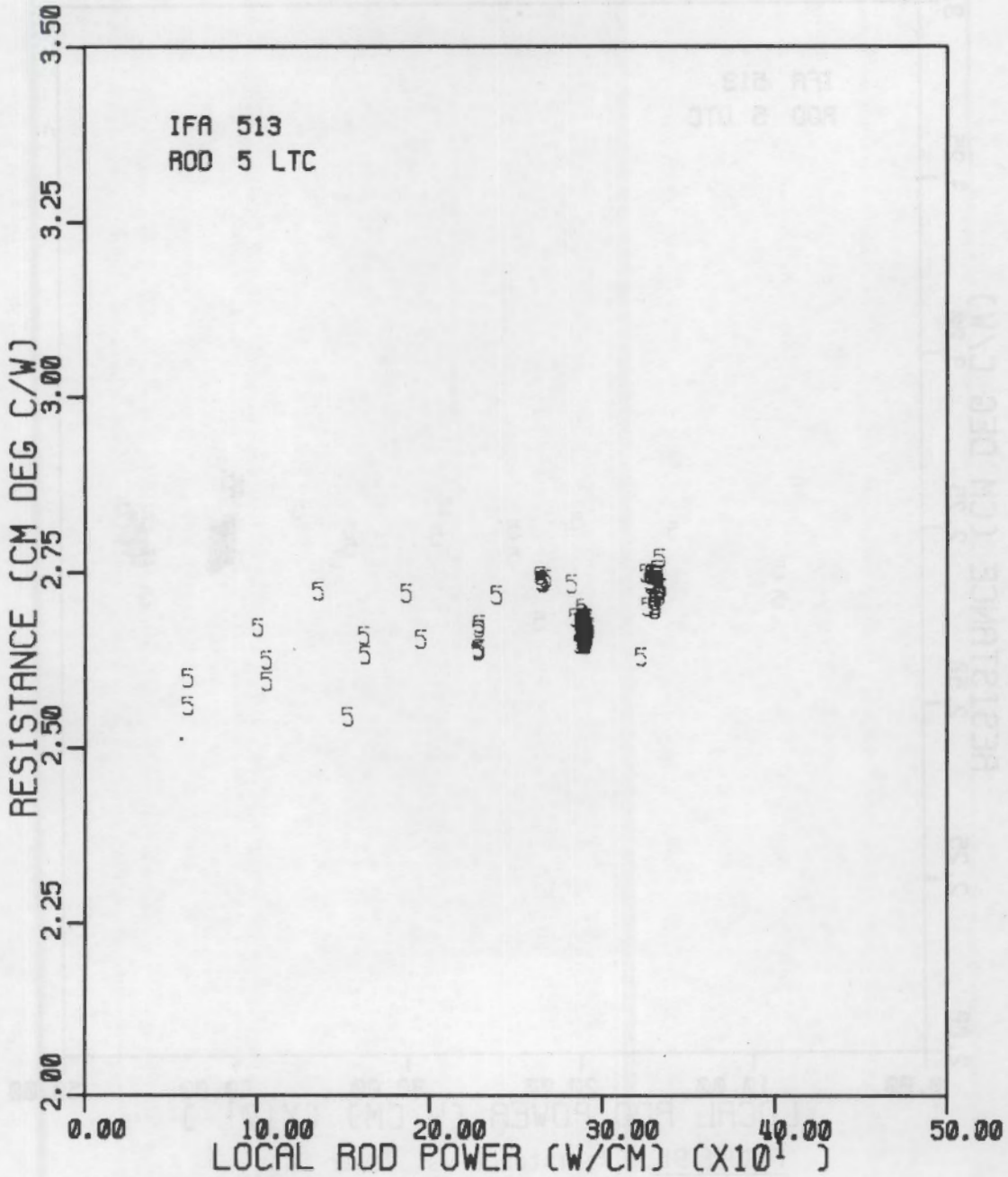

FIGURE 9a. Resistance vs. Power Data
For Rod 5, Lower Thermocouple.

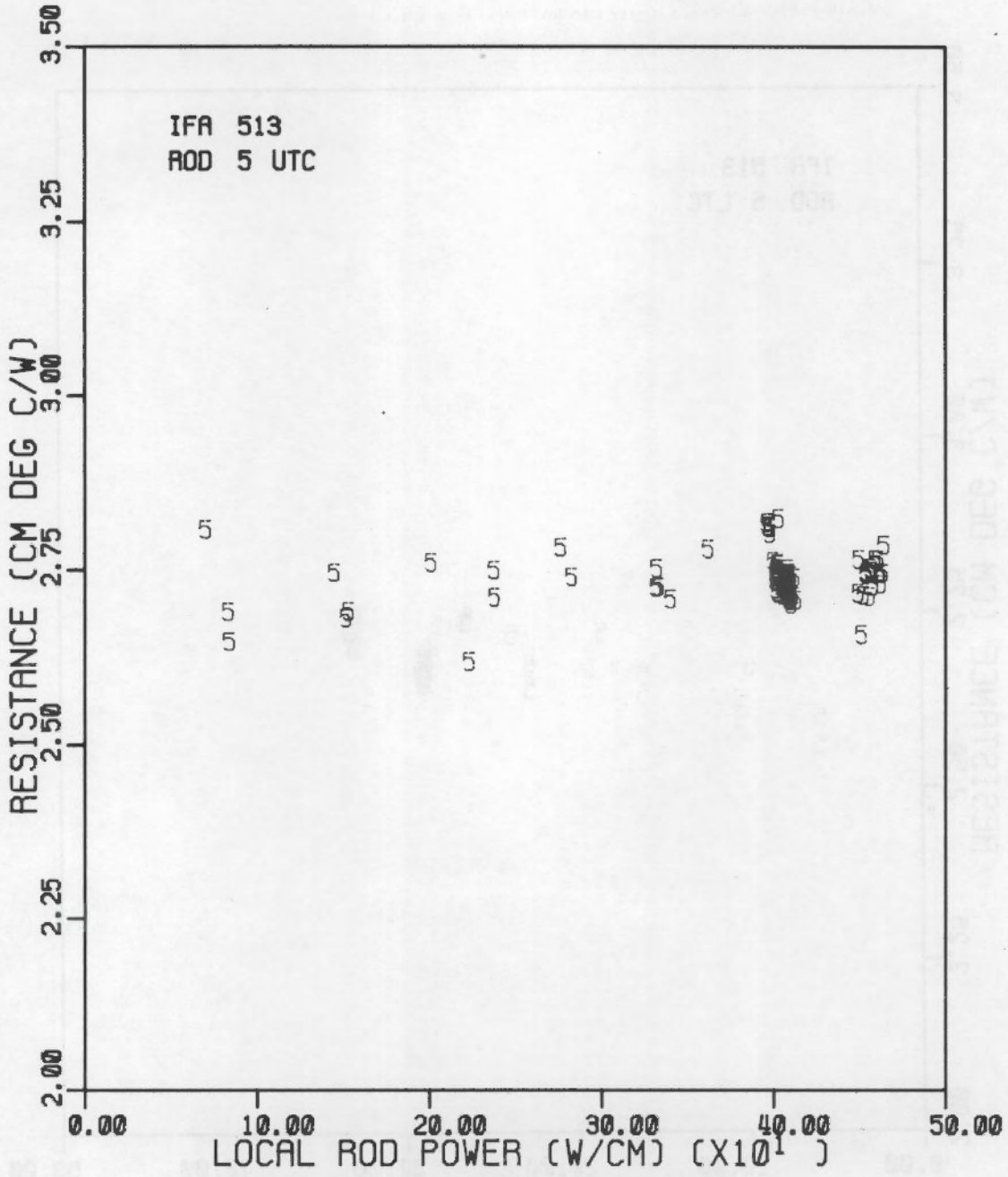

FIGURE 9b. Resistance vs. Power Data
For Rod 5, Upper Thermocouple.

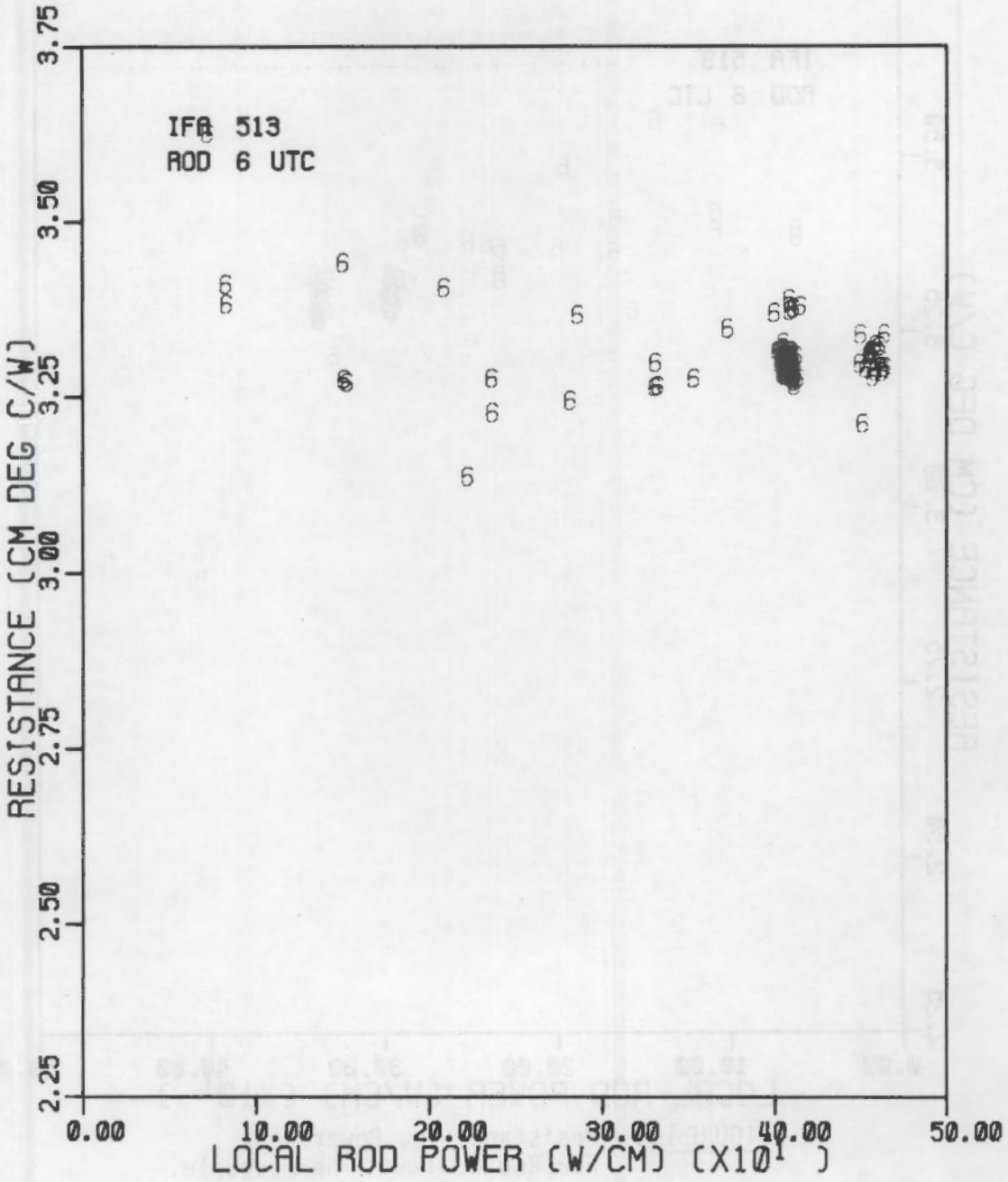

FIGURE 10a Resistance vs. Power Data
For Rod 6, Upper Thermocouple.

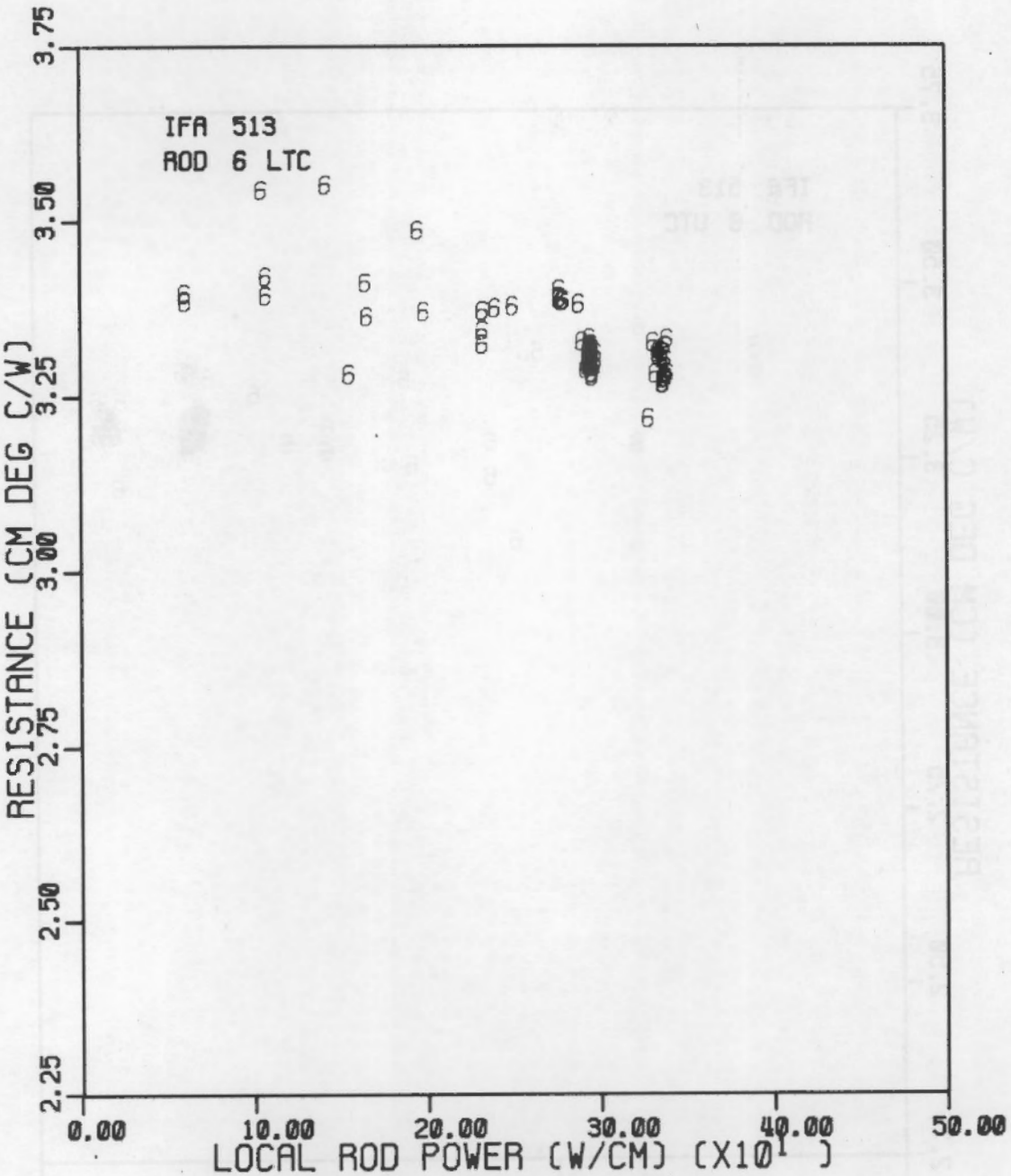

FIGURE 10b Resistance vs. Power Data
For Rod 6, Lower Thermocouple.

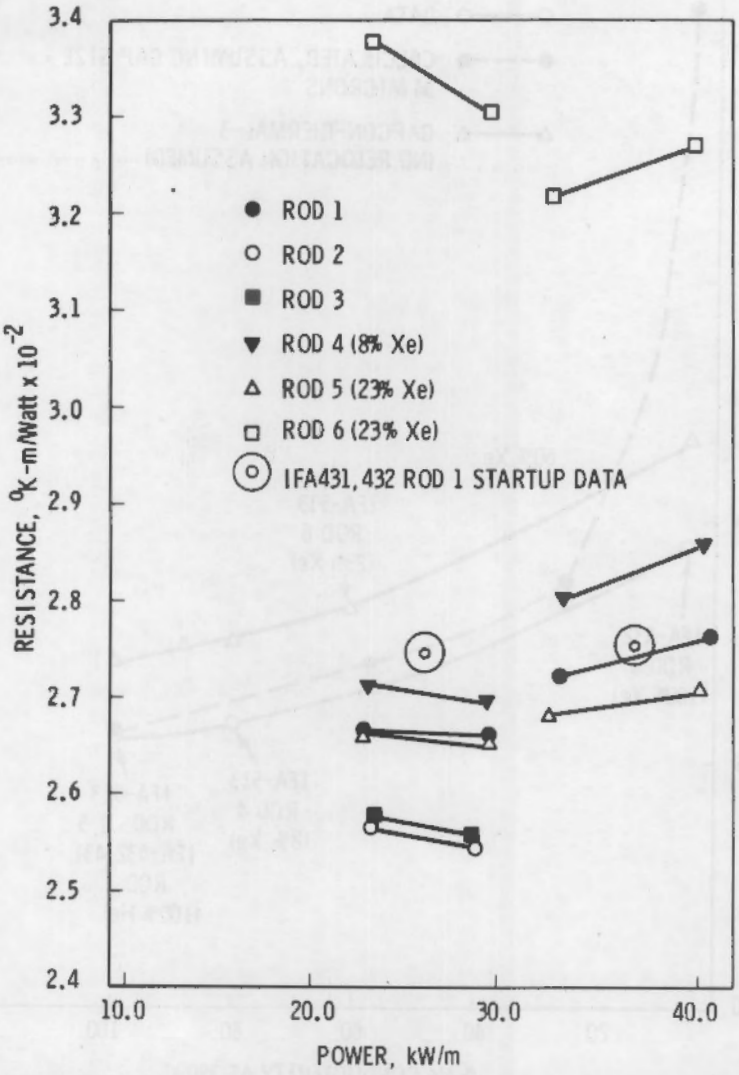

FIGURE 11 Resistance vs Power Data Trends for all Six IFA-513 Rods, Compared to the 230μ-gap, He-filled rods from IFA-431, -432

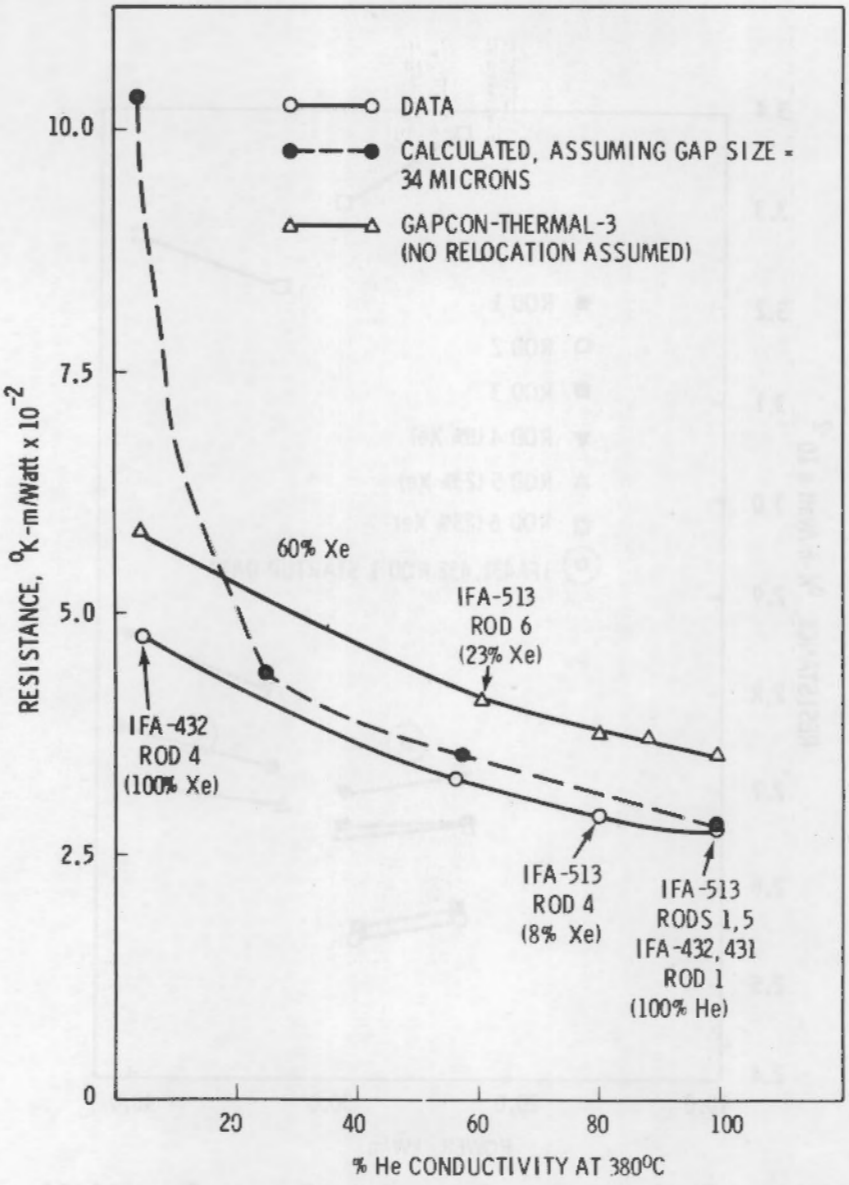

FIGURE 12. Resistance of IFA-513 and IFA-432 Rods (at 35 kW/m), as a Function of the Conductivity of the Fill Gas

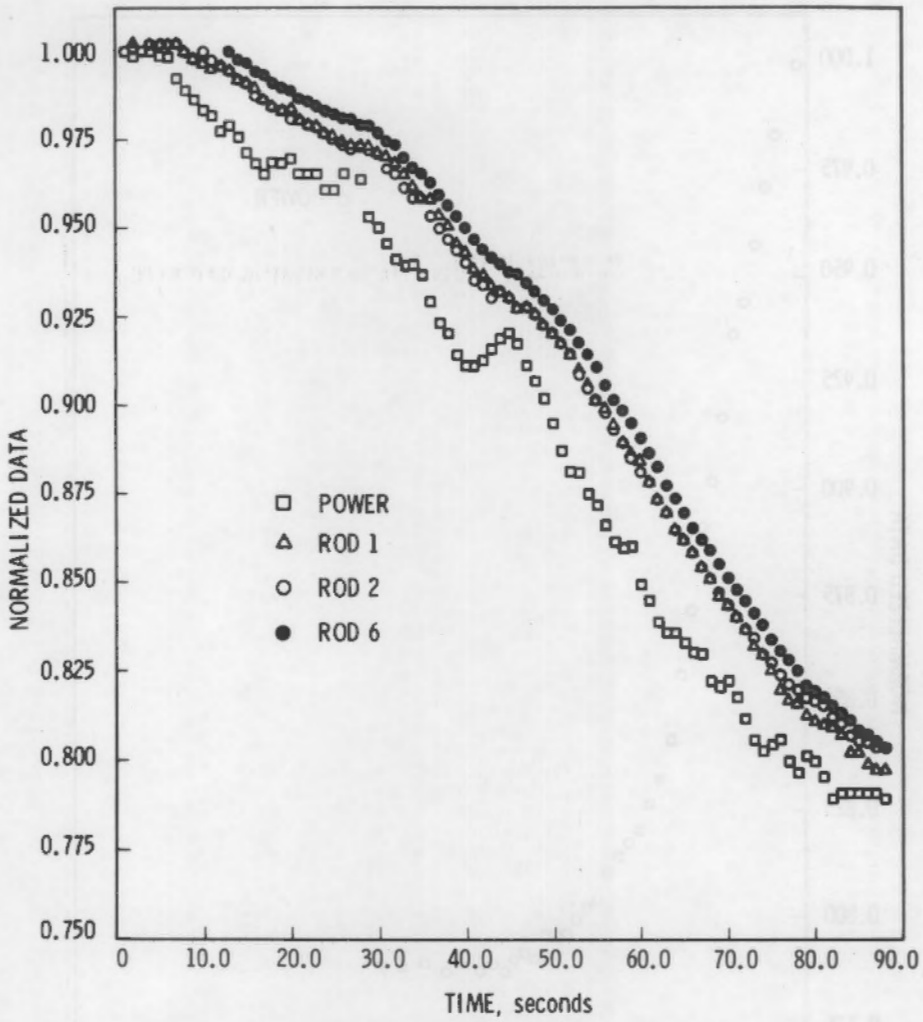

FIGURE 13. Power and Fuel Temperature Data for IFA-513 from Run 117 (a linear power decrease)

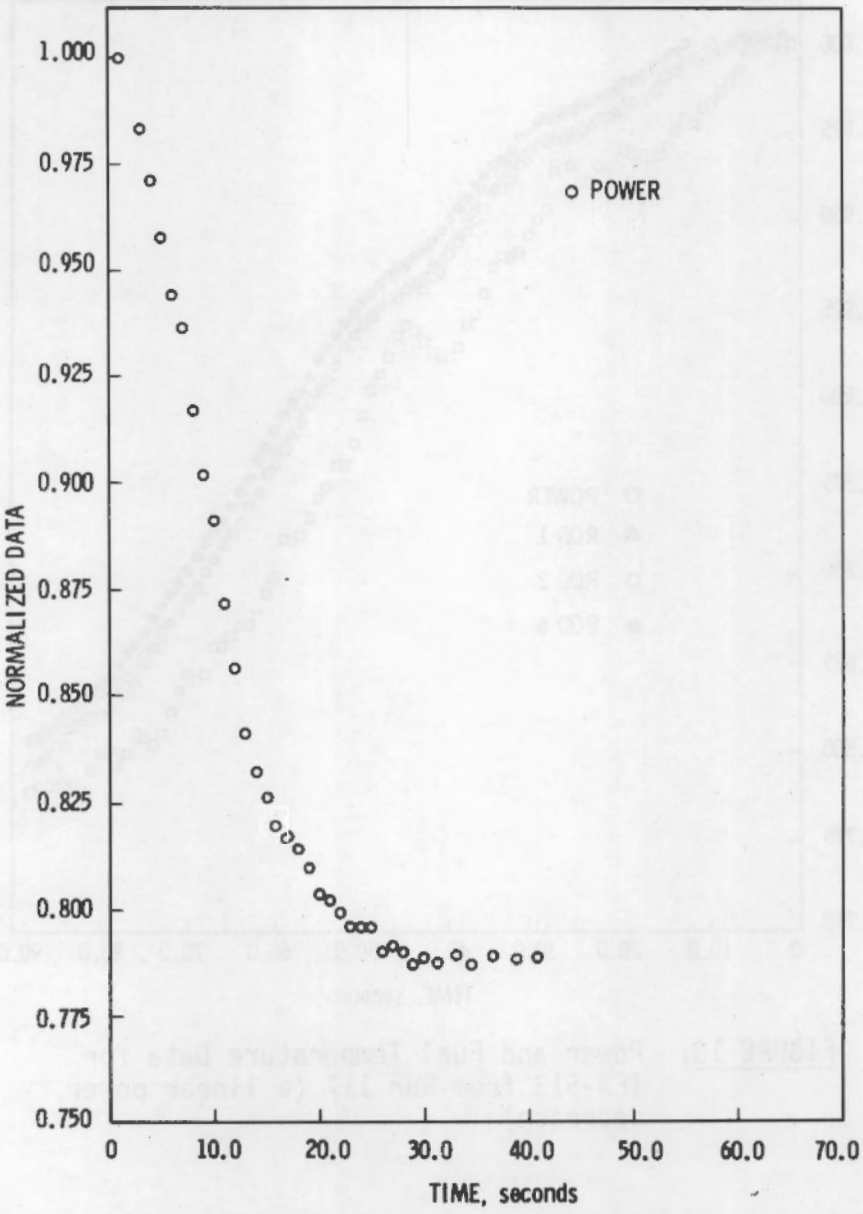

FIGURE 14. The Realtive Power Variation for Run 115 (a "step" Power Decrease)

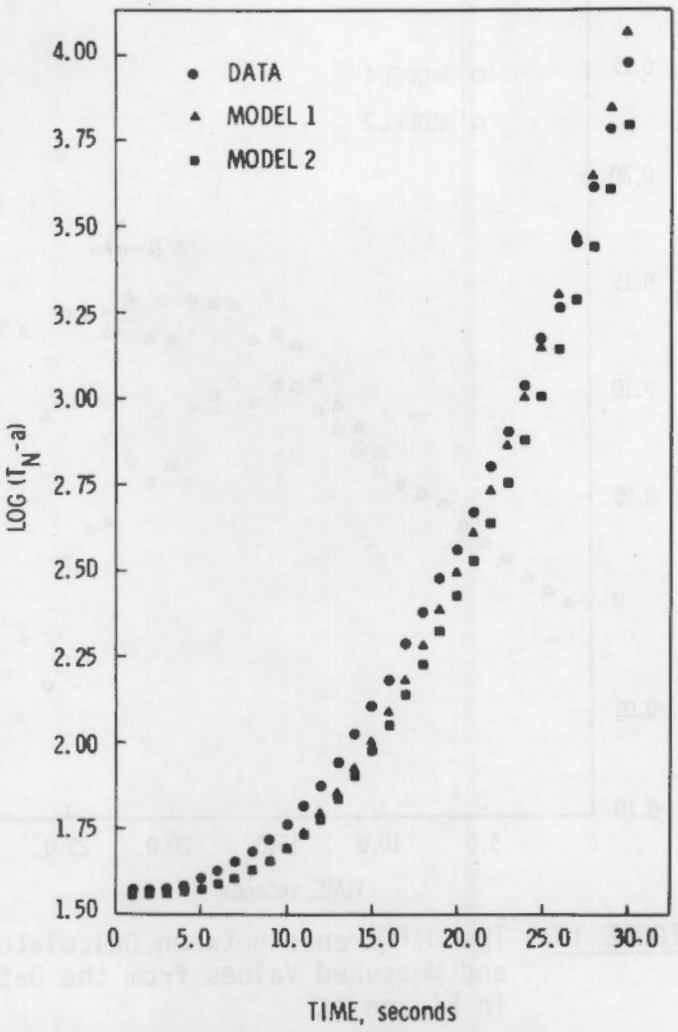

FIGURE 15. Data and Calculated Temperature Responses for the Upper Thermocouples of Rod 6 (Run 115)

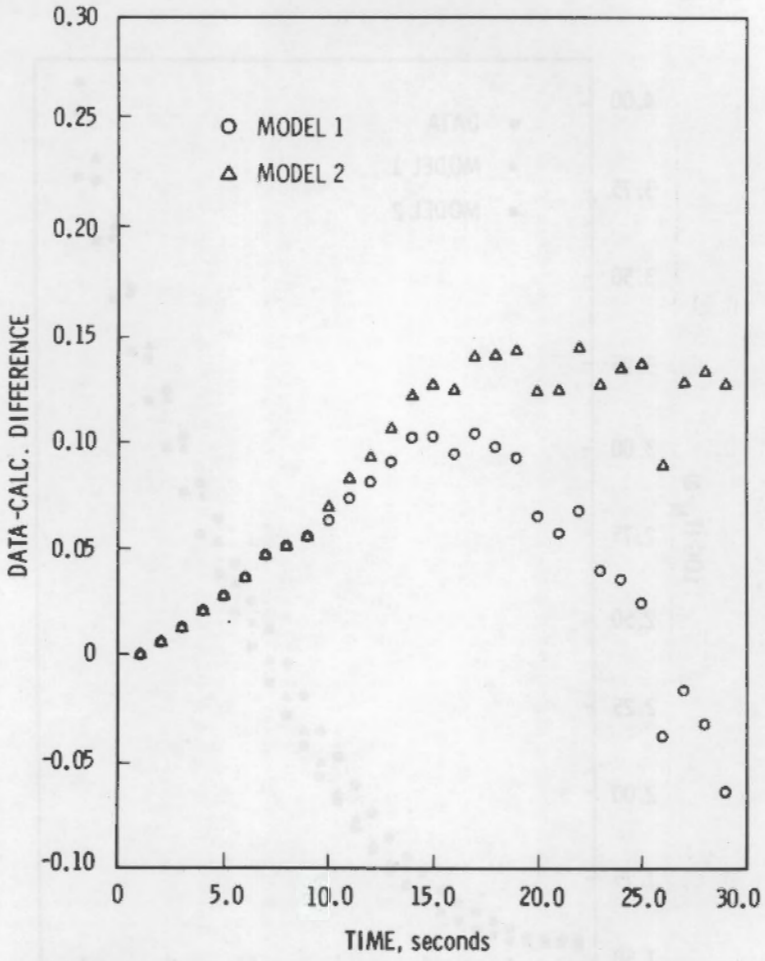

FIGURE 16. The Difference Between Calculated and Measured Values from the Data in Figure 15

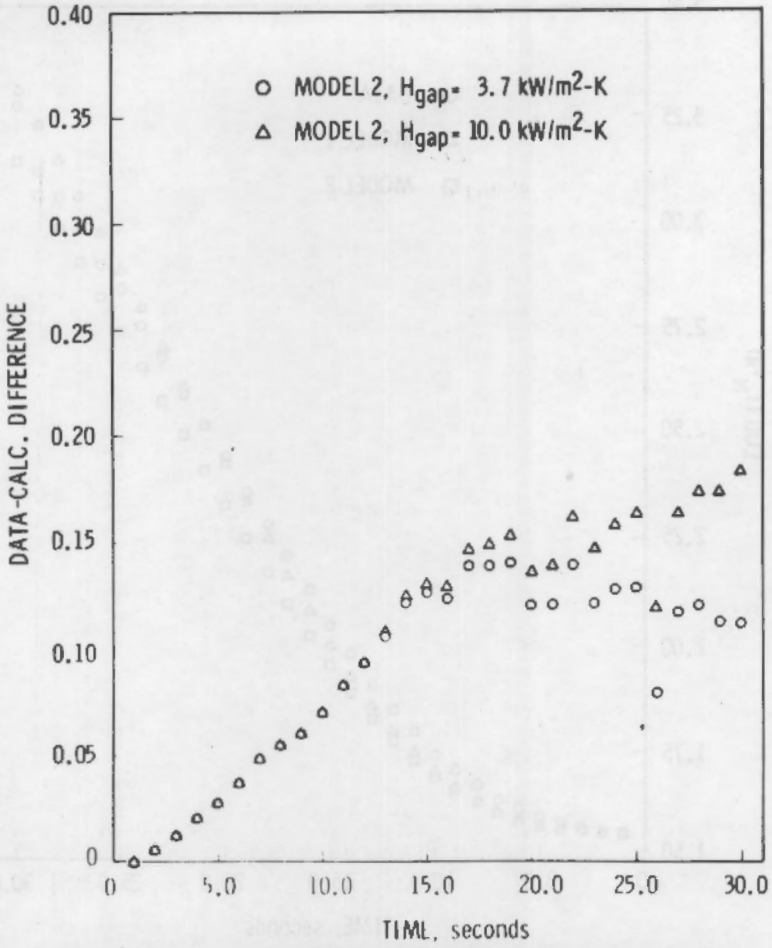

FIGURE 17. Calculated-Measured Difference for Model 2 Applied to Rod 6 (Upper) Run 115

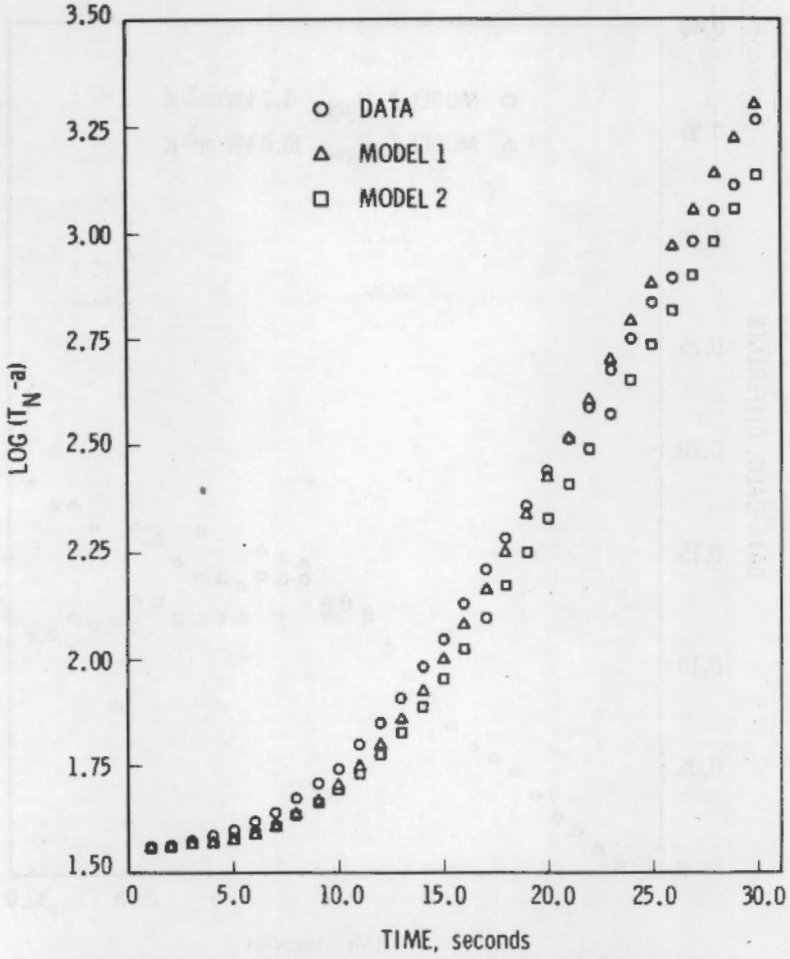

FIGURE 18. Data and Calculated Response for Rod 6 (Lower Thermocouple) Run 115

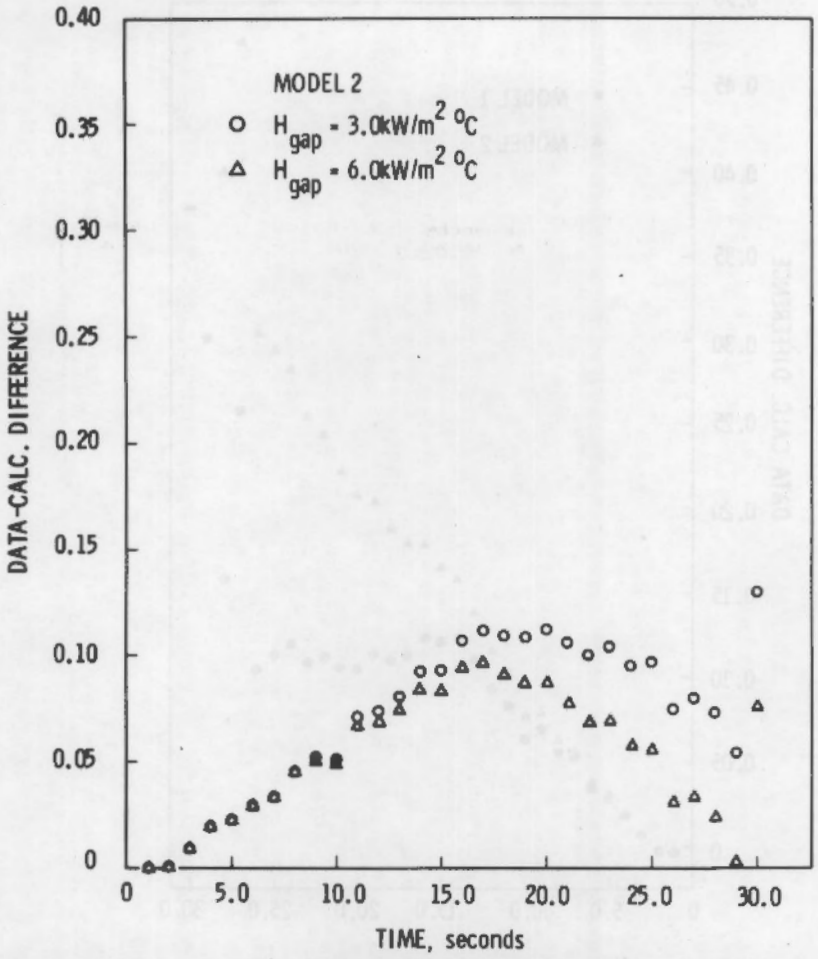

FIGURE 19. Calculated-Measured Difference for Model 2 Applied to Rod 6 (Lower) Run 115

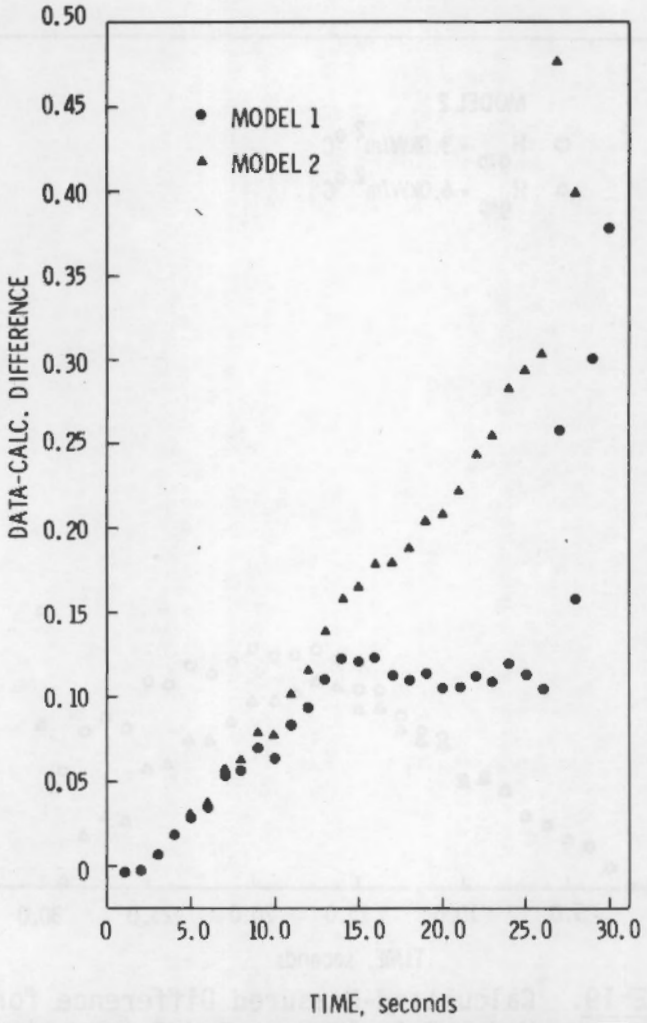

FIGURE 20. Calculated-Measured Differences for Models 1 and 2 Applied to Rod 1 (Lower Thermocouple) Run 115

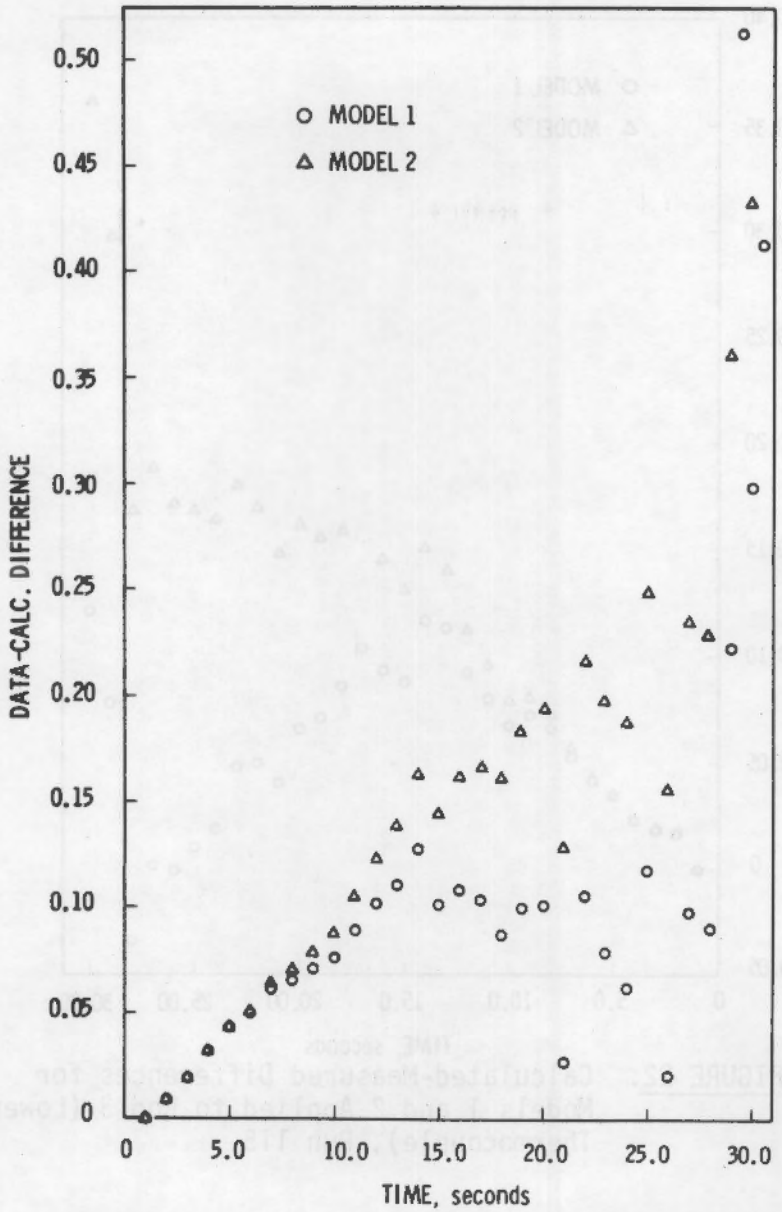

FIGURE 21. Calculated-Measured Differences for Models 1 and 2 Applied to Rod 2 (Lower Thermocouple) Run 115

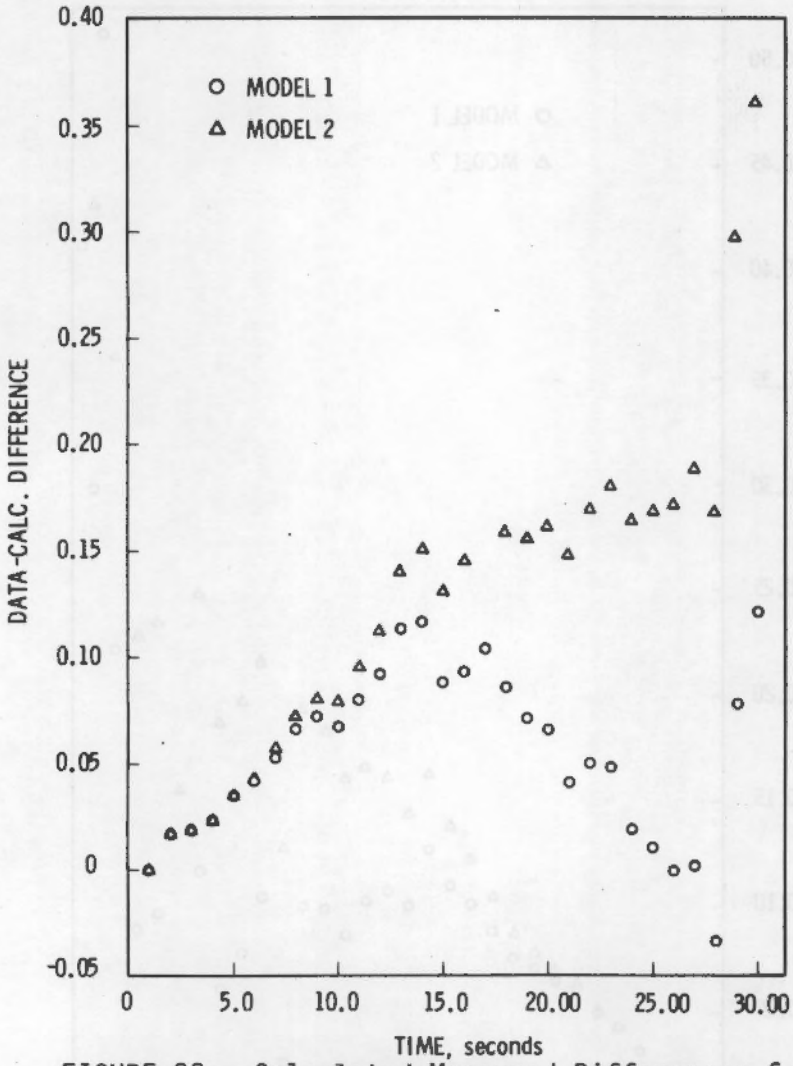

FIGURE 22. Calculated-Measured Differences for Models 1 and 2 Applied to Rod 3 (Lower Thermocouple), Run 115

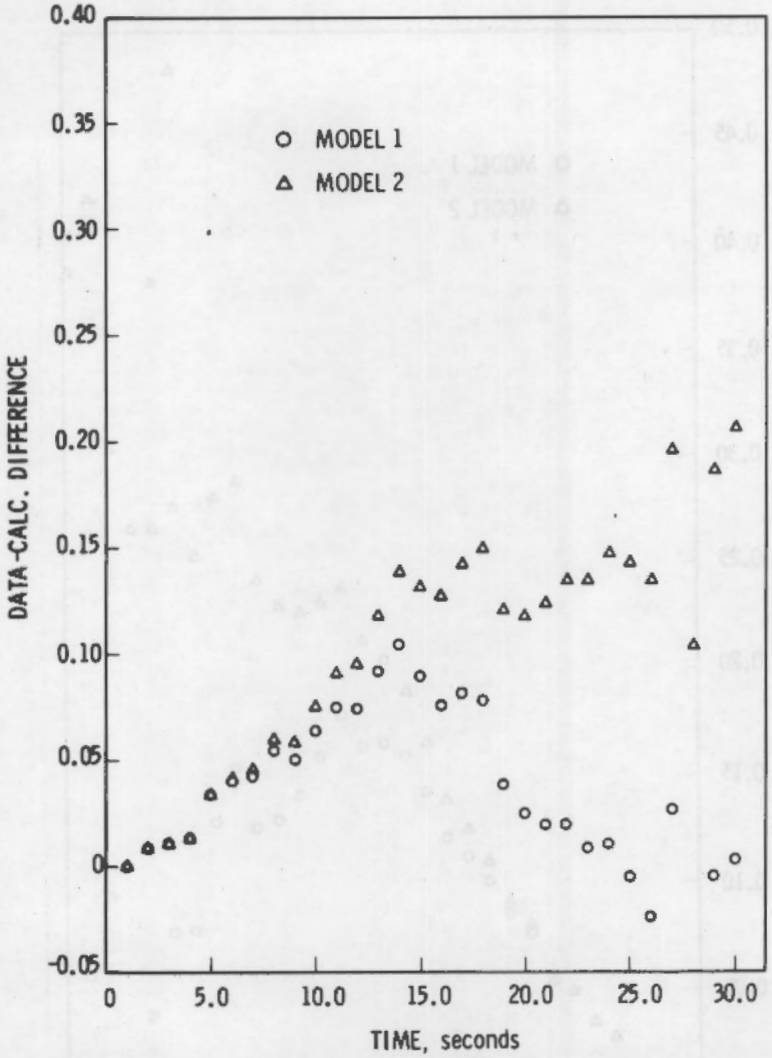

FIGURE 23. Calculated-Measured Differences for Models 1 and 2 Applied to Rod 5 (Lower Thermocouple) Run 115

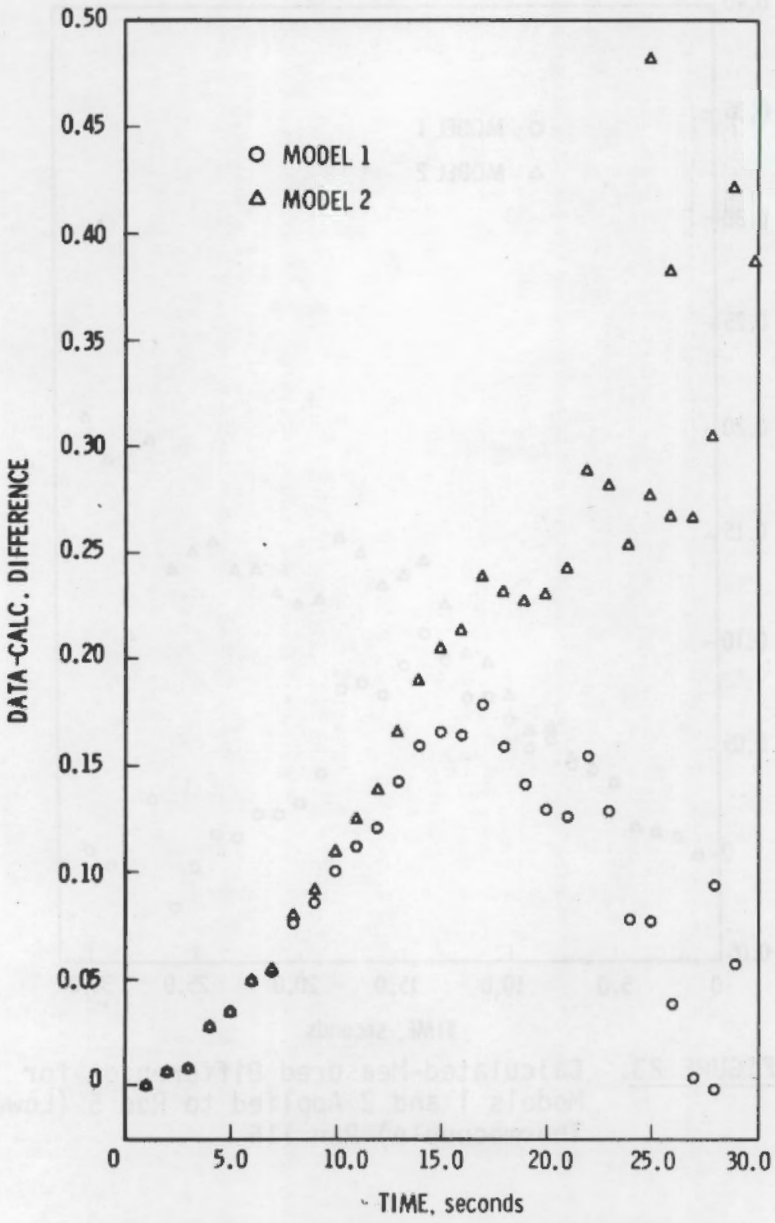

FIGURE 24. Calculated-Measured Differences for Models 1 and 2 Applied to Rod 1 (Upper Thermocouple) Run 115

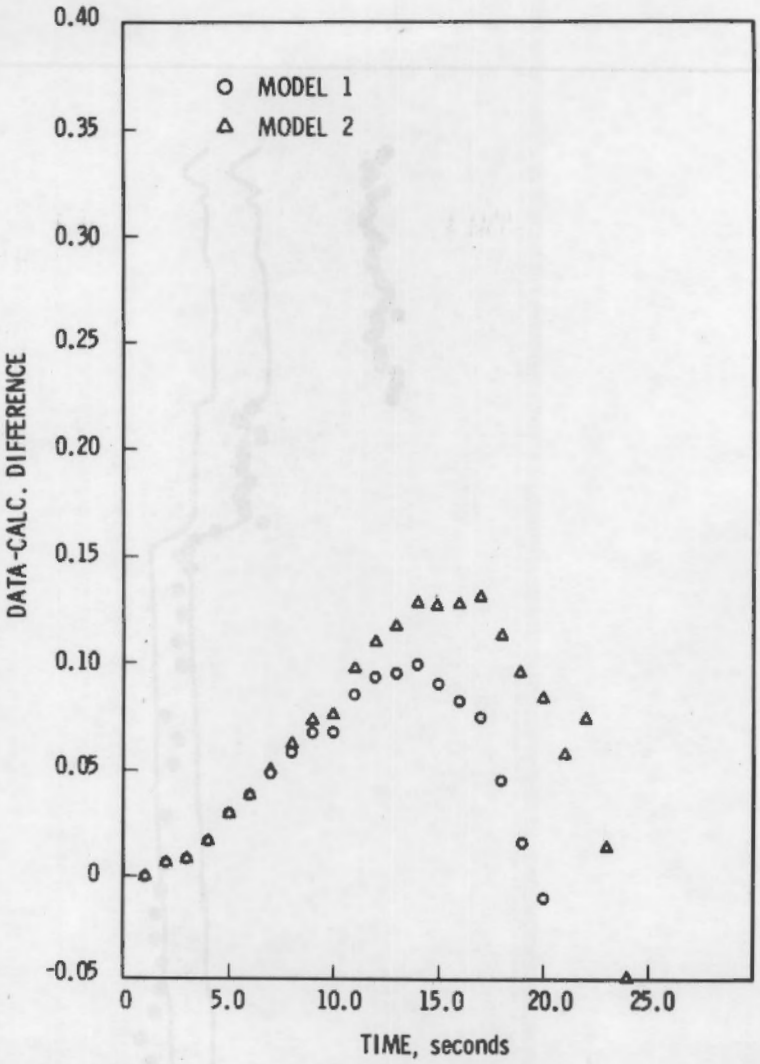

FIGURE 25. Calculated-Measured Differences for Models 1 and 2 Applied to Rod 5 (Upper Thermocouple), Run 115

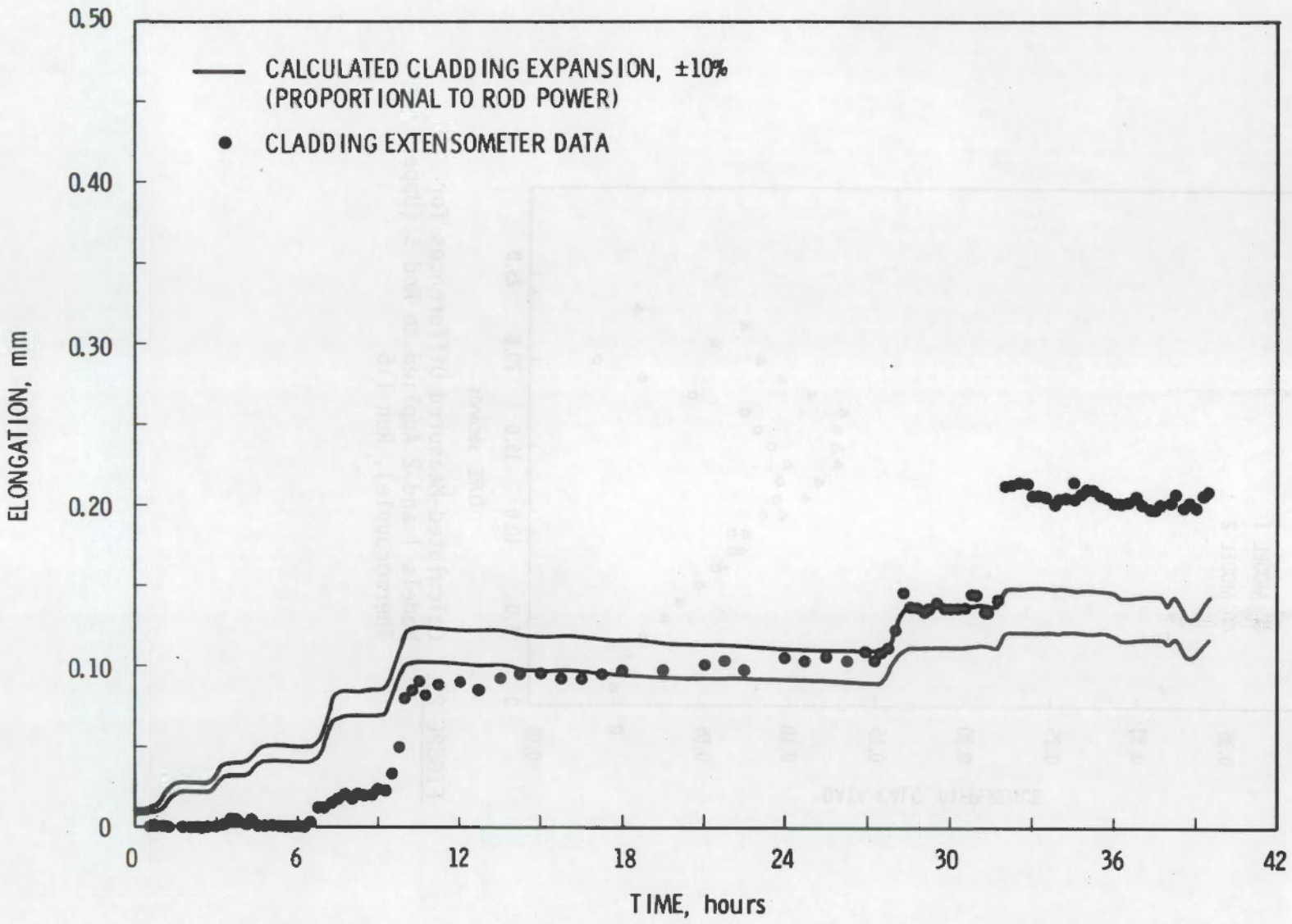

FIGURE 26. Cladding Elongation Data for First Power Ramp for Rod 1

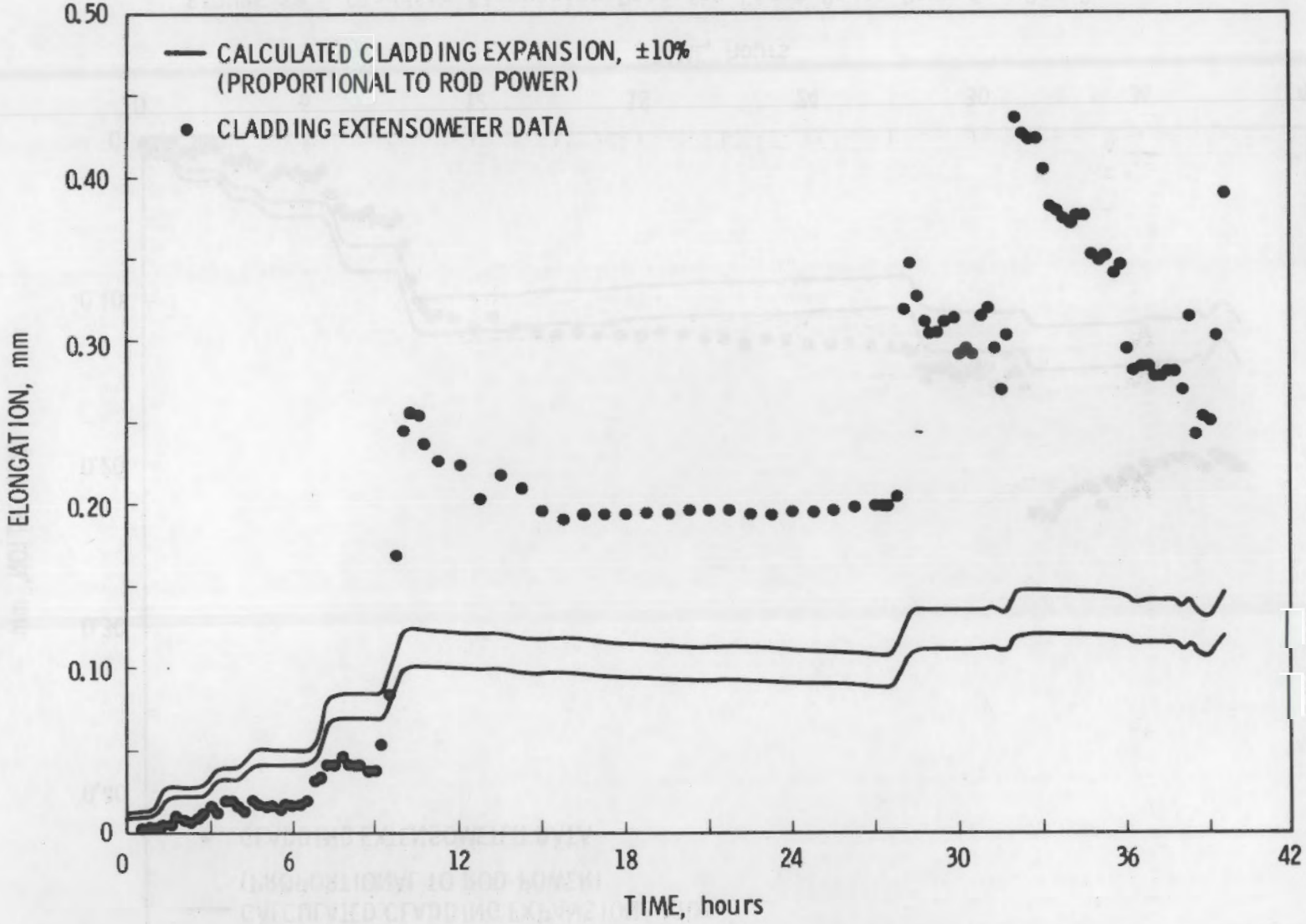

FIGURE 27. Cladding Elongation Data for First Power Ramp for Rod 2

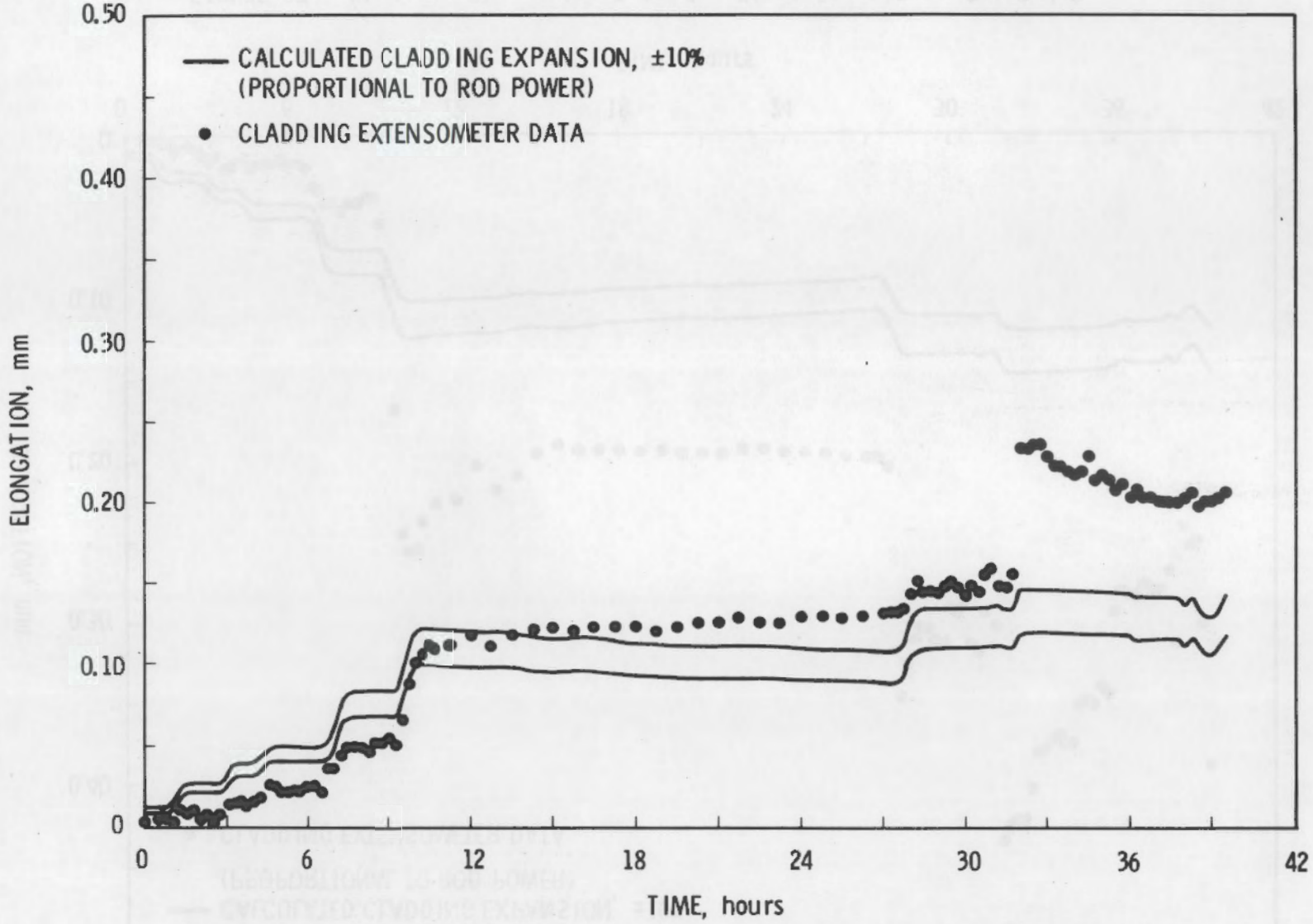

FIGURE 28. Cladding Elongation Data for First Power Ramp for Rod 3

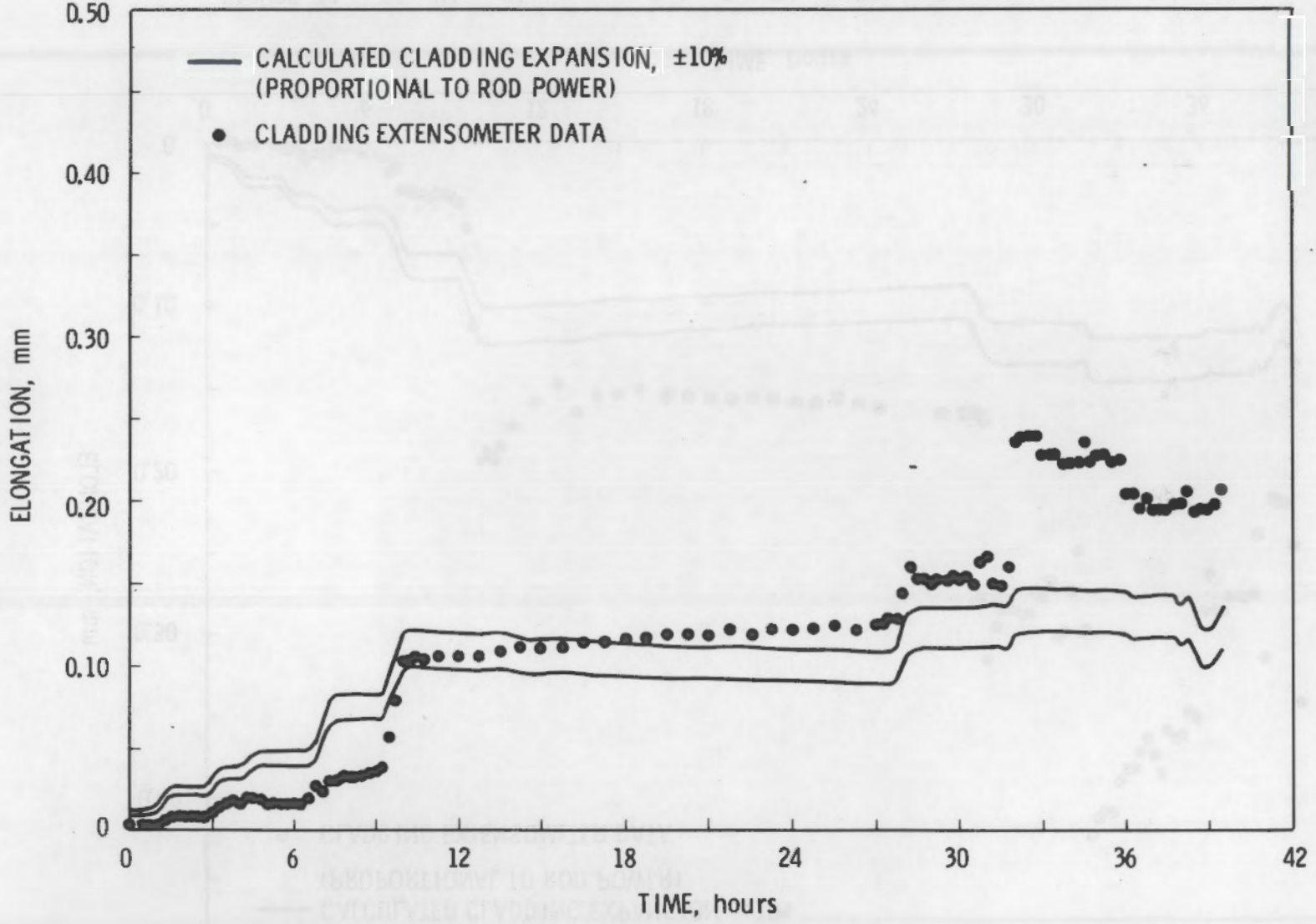

FIGURE 29. Cladding Elongation Data for First Power Ramps for Rod 5

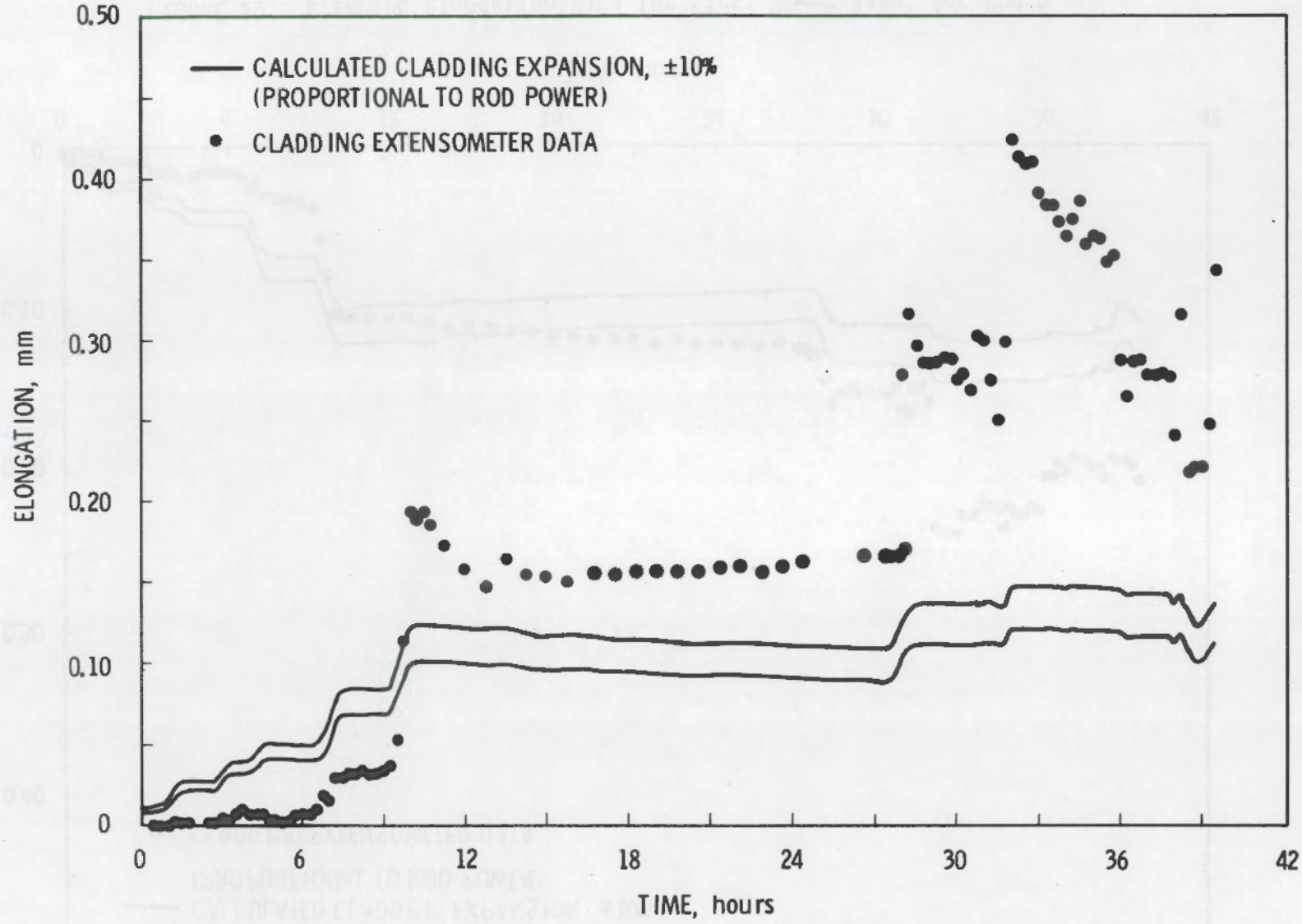

FIGURE 30. Cladding Elongation Data for First Power Ramp for Rod 6

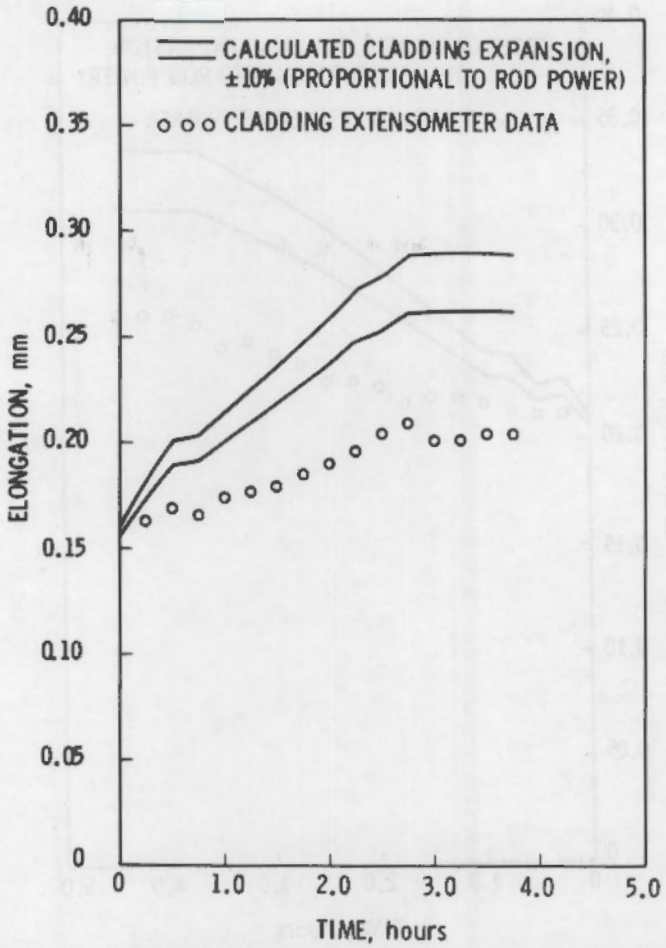

FIGURE 31. Cladding Elongation for Rod 1, Ramp 2

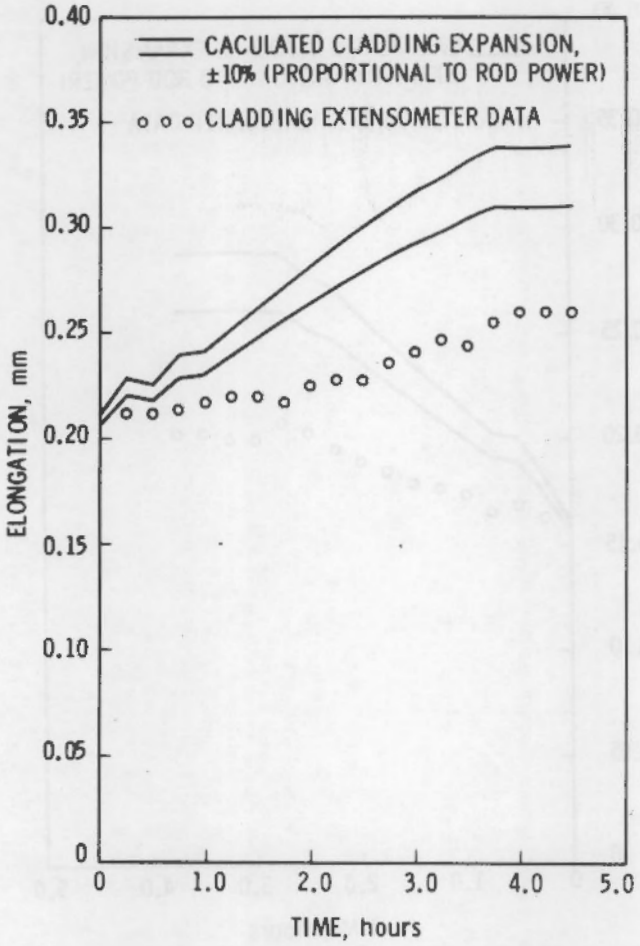

FIGURE 32. Cladding Elongation for Rod 1, Ramp 3

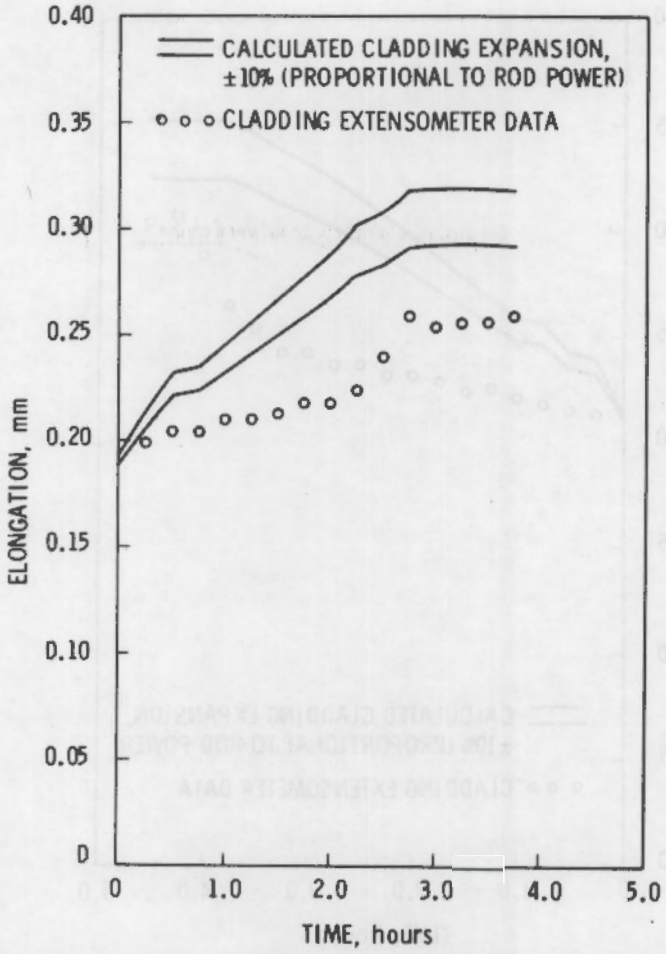

FIGURE 33. Cladding Elongation for Rod 6, Ramp 2

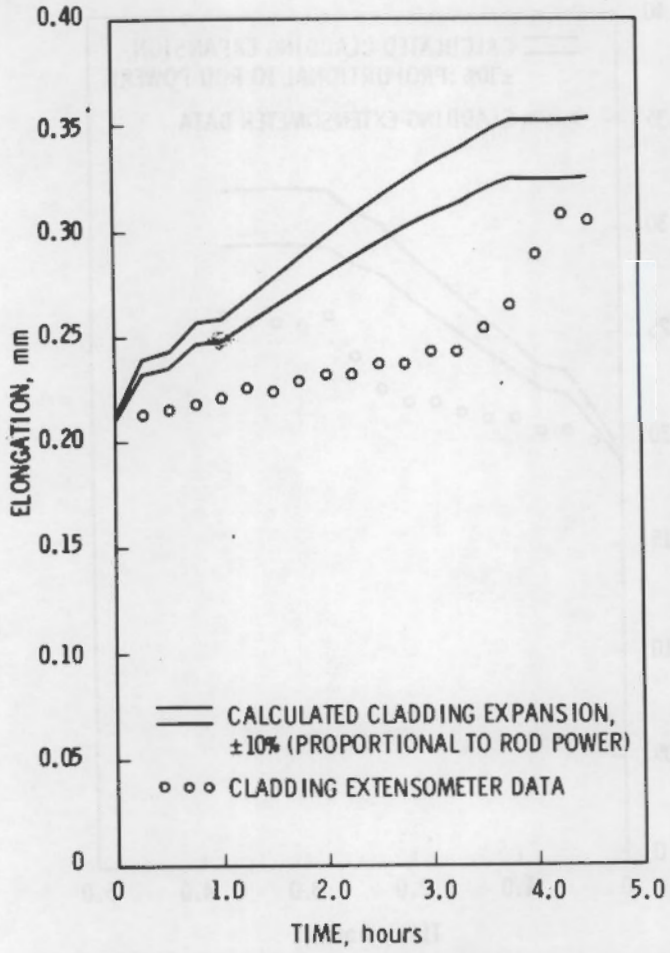

FIGURE 34. Cladding Elongation for Rod 6, Ramp 3

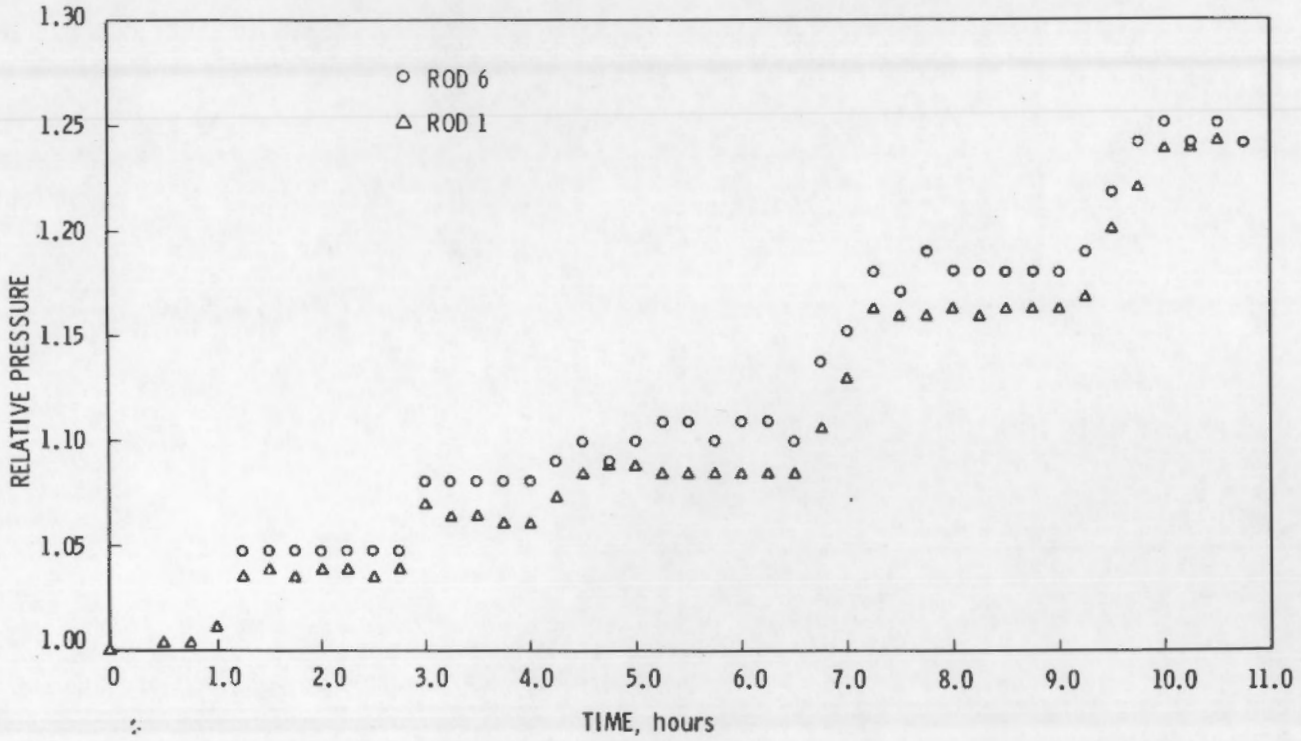

FIGURE 35. Gas Pressure Data (Relative to Zero Power Value) for Rods 2 and 6, From the First Power Ramp

ACKNOWLEDGEMENTS

The authors wish to thank the Fuel Behavior Research Branch, Office of Reactor Safety Research, Nuclear Regulatory Commission, for their continued support and encourgement of the experimental program. We also thank the Halden Reactor Staff for their efforts in recording and transmitting IFA-513 data. Special thanks is due to R. W. Miller, the NRC representative at Halden, for coordinating the special operating requests for IFA-513. Thanks also to Clarice Hagen who coordinated the typing and graphics for this report.

DISTRIBUTION

No. of Copies

OFFSITE

A. A. Churm
DOE Patent Division
9300 S. Cass Avenue
Argonne, IL 60439

287 Nuclear Regulatory Commission
Division of Technical Information and Document Control
7920 Norfolk Avenue
Bethesda, MY 20014

25 NTIS

2 DOE Technical Information Center

5 W. V. Johnston
Chief, Fuel Behavior Research Branch
Division of Reactor Safety Research
U.S. Nuclear Regulatory Commission
Washington, DC 20555

DNSITE

44 Pacific Northwest Laboratory

W. J. Bailey
J. O. Barner
S. Begej
E. R. Bradley
E. L. Courtright
M. E. Cunningham
M. D. Freshley
J. F. Garnier
R. L. Goodman
R. J. Guenther
C. M. Hagen
C. R. Hann (10)

No. of Copies

ONSITE

Pacific Northwest Laboratory (contd)

P. L. Hendrick
K. A. Hsieh
D. D. Lanning
R. K. Marshall
R. P. Marshall
C. L. Mohr
C. Nealley
F. E. Panisko
P. J. Pankaskie
W. N. Rausch
R. E. Schreiber
S. R. Wagoner
G. D. White
R. E. Williford
Technical Information (5)
Publishing Coordination (2)